Stripper Modification of a Standard MEA Process for Heat Integration with a Pulp Mill

PATY ARANGO MUÑOZ

Abstract

The 20 largest pulp mills in Sweden emit around 20 million tonnes of CO_2 per year. These emissions are considered carbon-neutral since they originate from biogenic sources. The pulp and paper industry is therefore a good candidate for the application of BECCS (Bioenergy with Carbon Capture and Storage) and has the potential to play a significant role for reaching the long-term mitigation target set by the Swedish government that Sweden should be climate-neutral by year 2045. In this thesis, a MEA-based chemical absorption and desorption process was rigorously modelled in Aspen Plus using the rate-based method.

Validation of the absorber and stripper model was conducted before the standard process was modified to a configuration that enables heat integration of a significant amount of excess heat from the capture process in, for example, a Kraft pulp mill. CO_2 removal rate and rich solvent loading were used as performance indicators to validate the absorber columns. The reboiler duty and lean solvent loading served as performance indicators in the stripper validation. The columns were dimensioned considering 90 wt% capture rate. Efficient use of the entire packing in the absorber and stripper columns was ensured by testing different solvent flow rates.

Suitable temperature levels for heat integration, within and across the capture plant, were obtained through an assessment of different versions of a stripper overhead compression configuration. The evaluation of the modified MEA processes took into account the steam conservation potential and energy efficiency potential. The simulation results indicate that the modified stripper may lead to savings of up to 11% in steam consumption. Heat integration between the capture plant and a specific process in a reference Kraft pulp mill resulted in energy savings of the same order of magnitude. Thereby, making the BECCS concept a more attractive solution for the Swedish pulp and paper industry to mitigate climate change.

Keywords
Carbon dioxide capture, pulp mill, chemical absorption, modelling, heat integration

Sammanfattning

De 20 största massabruken i Sverige släpper tillsammans ut ungefär 20 miljoner ton CO_2 per år. Dessa utsläpp har biogent ursprung och anses därför vara klimatneutrala. Massa- och pappersindustrin är därmed en lämplig kandidat för implementeringen av BECCS (eng. Bioenergy with Carbon Capture and Storage) och har en betydande potential att nå de, av den svenska regeringen, uppsatta klimatmålen som säger att Sverige inte ska några nettoutsläpp av växthusgaser till atmosfären senast år 2045. I detta examensarbete simulerades kemiska absorptions- och desorptionsprocesser med MEA som lösningsmedel genom att tillämpa den hastighetsbaserade metoden i en rigorös modell i Aspen Plus.

Stripper- och absorptionsmodellerna validerades innan standardprocessen modifierades till en konfiguration som möjliggör värmeintegration av koldioxidinfångningens överskottsvärme med, exempelvis, ett sulfatmassabruk. Avskiljningsgraden och laddning hos den mättade lösningen användes som prestandaindikatorer för att validera absorptionskolonnerna. Återkokarens energiåtgång och laddning hos den omättade lösningen användes som prestandaindikatorer för att validera stripperkolonnerna. Samtliga kolonner dimensionerades för att erhålla 90 vikt% avskiljningsgrad. Olika flödeshastigheter av lösningsmedlet testades för att säkerställa effektivt nyttjande av packningen i absorptions- och stripperkolonnerna.

Lämpliga temperaturnivåer för värmeintegration, inom och utanför, koldioxidinfångningen erhölls genom att utvärdera olika varianter av en stripper-overhead-kompression konfiguration. Utvärderingen av den modifierade MEA processen tog hänsyn till potentialen för ångbesparing och energieffektivisering. Resultat från simuleringarna tyder på att den modifierade strippern skulle kunna ge besparingar på upp emot 11 % i ånganvändning. Energibesparingar i samma storleksordning kunde även erhållas genom värmeintegration mellan koldioxidinfångningen och en särskild process i ett referensbruk. Implementering av BECCS-konceptet på det här sättet skulle därmed kunna bli ett mer attraktivt alternativ för den svenska massa- och pappersindustrin att bekämpa klimatförändringarna.

Nyckelord
Koldioxidinfångning, massabruk, kemisk absorption, modellering, värmeintegration

Acknowledgments

Contents

Nomenclature

Abbreviations

ADt	Air dry tonne
BECCS	Bioenergy with Carbon Capture and Storage
CCS	Carbon Capture and Storage
CSTR	Continuous Stirred-Tank Reactor
DCC	Direct Contact Cooler
dP	Pressure drop
DS	Dry Solid
ENRTL-RK	Electrolyte Non-Random Two Liquid with Redlich-Kwong thermodynamic model
GMENCC	Aspen Plus ENRTL interaction parameters for molecule-ion and ion-ion pairs
$GtCO_{2e}$	Gigatonnes of equivalent carbon dioxide
H/D	Height to diameter ratio
IEA	International Energy Agency
IPCC	Intergovernmental Panel on Climate Change
L/G	Liquid to gas ratio
L_{min}	Minimum lean solvent flow rate
NCG	Non-Condensable Gases
Post-CC	Post-Combustion Capture
PSRK	Predictive Soave-Redlich-Kwong equation of state model
RISE	Research Institutes of Sweden
SINTEF	Foundation for Scientific and Industrial Research at the Norwegian Institute of Technology
TRL	Technical Readiness Level
TRS	Total Reduced Sulfur
t_{CO2}	Tonne CO_2 captured
UTA	University of Texas at Arlington

Chemical compounds

AMP	2-amino-2-methyl-1-propanol
CO_2	Carbon dioxide
H_2O	Water
K_2CO_3	Potassium carbonate
MDEA	Methyldiethanolamine
MEA	Monoethanolamine
NH_3	Ammonia
NO_2	Nitrogen dioxide
O_2	Oxygen
PZ	Piperazine
SO_x	Sulfur oxides
SO_2	Sulfur dioxide
SO_2	Sulfur trioxide

1. Introduction

One of the most frequently used processes for CO_2 capture from flue gases is alkanoamine scrubbing as it has been known since the beginning of the 20th century (Hammer et al., 2006) and is currently used in several industry processes, such as natural gas sweetening, ammonia production and syngas upgrading and synthesis. However, the principal aim of the CO_2 capture in the early years was the separation of the CO_2 to upgrade the natural gas found in reservoirs for commercial purposes. The use of this technology for emission reductions in the process industry with the purpose of tackling the greenhouse effect was first proposed in the 1970's. Although, it was not until recent years that the carbon capture and storage (CCS) concept started to attract an increasing number of large project initiatives.

The Swedish government has set the long-term climate goal that Sweden should be climate-neutral by year 2045 (Regeringskansliet, 2017). Some interesting large point sources of CO_2 emissions in Sweden with respect to CCS are industries such as pulp and paper, integrated steel mills, oil refineries, cement and chemical production plants. Most of the attention for CO_2 abatement has nonetheless been towards the fossil-fueled industries and much less on the pulp and paper industry. The CO_2 emissions from pulp and integrated pulp and paper mills in this heavily industrialized region originate from biogenic sources, thus considered carbon-neutral (Garðarsdóttir, 2017). This industry is therefore a good candidate for the application of BECSS, a concept that combines bioenergy with CCS, especially since a conventional pulp mill emits millions of tonnes of CO_2 per year (Global CCS Institute, 2011).

1.1. Aim

The main objective of the thesis is to build a rate-based model of an amine-based absorption/desorption process for CO_2 capture in Aspen Plus. Another objective is to evaluate the possibility to integrate excess heat from a modified capture process in, for example, a Kraft pulp mill. However, due to patent pending by RISE, the content of this report will neither disclose which of the reference pulp mill processes is considered for such an integration scenario nor present any quantitative information relating to the needed customization of the processes involved. The thesis objectives were accomplished through:

- Validation of the absorber and stripper model by comparing simulations results with data from four different experimental trials that were found in literature.
- Modification of the capture process by adding one vapor compression step in the stripper reflux.
- Calculation of performance values, e.g. heat duty, and resulting heat temperature levels in the standard and modified MEA processes.
- Evaluation of the energy saving potential in a heat integration scenario between an energy intensive pulp mill process and the carbon capture plant.

2. Carbon capture

By the end of 2019, over 260 million tonnes (Mt) of CO_2 emissions from anthropogenic sources have already been captured and permanently stored. Most of the injected CO_2 was used to increase oil production through enhanced oil recovery. 40 Mt per year is the approximate global capture and storage capacity of large-scale CCS facilities that are currently operating or under construction. Although, if including the facilities at earlier stages of development the total number of large-scale facilities would add up to 51; accordingly, their capture and storage capacity is around 98 Mt per year. The largest share of CO_2 captured from these plants all together originates from either coal fired power plants, natural gas processing or coal gasification plants. In addition to these larger projects, there are 39 pilot and demonstration scale CCS facilities (Global CCS Institute, 2019). In the general case, BECCS has been recognized at an international level, e.g. in reports published by the IEA and IPCC respectively, for being the only large-scale technology capable of removing CO_2 from the atmosphere (ZEP & EBTP, 2012).

2.1. Bioenergy with CCS

The term "closed carbon loop" concerns the view of biomass as a carbon-neutral energy source by assuming that the equivalent amount of CO_2 released during the energy use of biomass is captured from the atmosphere during its growth. Concerns that the likelihood of achieving the required safe atmospheric CO_2 stabilization level is diminishing with every passing year has driven the attention towards carbon-negative energy systems. Bioenergy with CCS falls under the definition of such systems, which enable a greater amount of atmospheric CO_2 to be absorbed and sequestered by the system than the CO_2 amount that would ultimately be released back to the atmosphere if not removed from the natural cycle (Muradov, 2014). The prerequisite for this notion to be valid is that the biomass is managed in a sustainable way (Onarheim et al., 2017). More specifically, the concept of BECCS refers to the capture of CO_2 released, through combustion or processing, at biomass point emission sources as well as the transport and injection of it into deep underground in geological formations for permanent storage. Not only can the recapturing and permanent storage of CO_2 with this approach lead to negative CO_2 emissions (Figure 1) but it also enables mitigation of carbon emissions that have already occurred (Global CCS Institute, 2011).
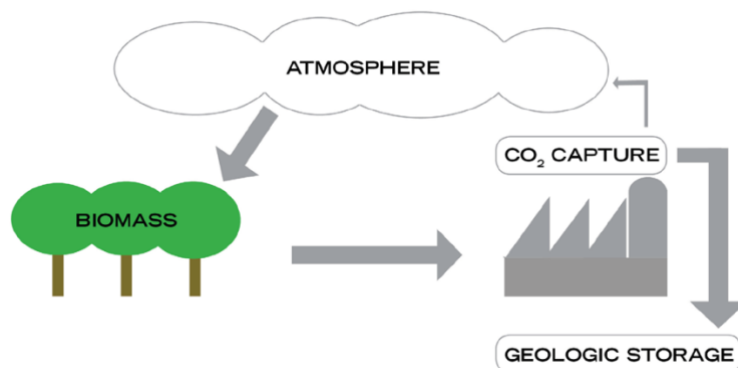
Figure 1 Illustration of how emissions that have already occurred can be mitigated by biomass fueled industrial plants employing the BECCS concept (Global CCS Institute, 2011).

The use of BECCS in several model studies was reported in the Fifth Assessment Report of IPCC (2014) in which several scenarios of pathways are taken into consideration to achieve climate stabilization at 2°C above pre-industrial levels. This report revealed the full range of potential climate impact of BECCS systems as 0-22 Gt of negative CO_2 emissions per year in 2100, where the largest potential corresponds to scenarios with the highest mitigation ambition consistent with a 2°C target (Smith & Porter, 2018). The mean level of the overall potential for BECCS was estimated at around 12.1 $GtCO_{2e}$/year (Fuss et al., 2016). Although, more realistic estimates through cautious assumptions in regard to a sustainable supply of biomass suggest a much lower removal capacity of BECCS: 3.3-7.5 $GtCO_{2e}$/year (Mclaren, 2012). Furthermore, the emission consequences between different BECCS technologies can differ as the amount of sequestered CO_2 may vary along the supply chain and the bioenergy may substitute different technologies (Fuss et al., 2016); for example, co-firing fossil fuels with 30% biomass requires a larger geological storage capacity when compared to the corresponding co-firing fossil fuels with 50% biomass (Mclaren, 2012).

2.2. Carbon capture technologies

Aqueous amine solutions, the most common among chemical absorption technologies, have been used to remove CO_2 from natural gas for several decades (Bottoms, 1931). Two large-scale coal fired plants that employ an amine-based system for post-combustion capture (Post-CC) are the Boundary Dam in Canada and the Petra Nova in the United States. Therefore, amine-based solvents are considered to have a technical readiness level (TRL) of 9 when implemented in power plants with post-combustion capture (Bui et al., 2018). With just three years in between their respective commissioning, the cost per t_{CO2} (tonne CO_2 captured) reduced from over $100 at the Boundary Dam to below $65 at the Petra Nova. Furthermore, most recent studies estimate the corresponding cost for facilities planning to start their operation in 2024-2028 at around $43 (Global CCS Institute, 2019). All this indicates that the more frequent the commissioning of mature carbon capture systems for industrial facilities becomes the more cost-feasible capture systems can be expected in the near future.

Among the most recent developments in polymeric membranes, the commercially available Polaris membrane has achieved TRL 7 and if its projected implementation goes as planned it may reach TRL 8 next year already (Batoon et al., 2019). Moreover, it has proven successful when used in post-combustion systems for CO_2 separation from syngas (MTR, n.d.). The suitability and selection of a capture technology will depend on the specific stream properties of any industrial process, such as moisture content and CO_2 concentration. This matter is specially addressed in a study (Hasan et al., 2012) that evaluated both an absorption process and a membrane process over a range of feed compositions and flow rates. Capture processes that include either membrane or adsorption require a moisture content of 0.1% or less to circumvent reduced CO_2 recovery and corrosion problems, respectively. On the other hand, absorption-based processes can tolerate a feed saturated with H_2O and will therefore handle a high moisture feed much better. The lower concentration of CO_2 the more capital and energy intensive separation process of the gas. Operation under oxidizing atmosphere may shorten the life of chemical solvents used in gas separation units (Muradov, 2014).

After having covered the necessary technological requirements for the capture process of CCS projects, their success will also depend on the availability of safe geological storage for the captured CO_2. Other factors that can help bring such projects into the operation phase

comprise supportive policy, legislative frameworks and secure financial funding (Bui et al., 2018). Unfortunately, negative carbon emissions are currently not taken into account in the European Union Emissions Trading System (Onarheim et al., 2017). Despite the non-existent incentives for implementation of CCS technologies in the pulp and paper industry, several studies have been published on this research topic in recent years. The extra energy demand needed for the capture process was assessed in a study (Hektor, 2008) in which a comparison of two different absorbents, monoethanolamine (MEA) and chilled ammonia, also was done. As different configurations for the energy supply were considered, it was concluded that an increasing degree of heat integration can be profitable for pulp and paper mills when choosing chilled ammonia over MEA as the solvent. The study also denoted that post-combustion capture of CO_2 can be economically feasible for the pulp and paper industry under certain favorable market conditions.

2.3.   Amine absorption

Amine-based absorption is the most commonly used process in Post-CC projects for gas cleanup. A series of advanced amines with improved stability and properties have been developed with the aim of lowering stripping steam requirement and enabling their use in power plants with thermal integration of carbon capture systems: sterically hindered amines (KS-1, KS-2 and KS-3), 2-amino-2-methyl-1-propanol (AMP), Cansolv and HTC Purenergy. The main challenges to the amine-based carbon capture systems when applied to Post-CC are associated with large parasitic loads due to: heating required for the absorbent regeneration, pumping of solutions and compressing of the gas to pipeline pressure (Muradov, 2014). The capital and operating costs of CO_2 capture processes with sorbents are largely dictated by their kinetic and thermophysical properties. The chemical absorbent MEA has become the benchmark amine for CO_2 capture from electricity generation due to its particular suitability for low CO_2 partial pressure applications (Bui et al., 2018).

Table 1 Energy consumption for various carbon capture absorbents, including single amine and amine blends, based on a standard absorber/stripper process configuration. The duty marked with asterisk (*) is calculated through simulation (Bui et al., 2018).

Solvent	Reboiler duty (GJ/t_{CO2})
30 wt% MEA	3.6–4.0
40 wt% MEA	3.1–3.3
40 wt% piperazine (PZ)	2.9
Cansolv	2.3
28 wt% AMP + 17 wt% PZ	3.0–3.2
MEA + MDEA (variable mix ratio)	2.0–3.7
Aqueous ammonia (NH_3)	2.0–2.9*
Aqueous potassium carbonate (K_2CO_3)	2.0–2.5

Using 30 weight percent (wt%) MEA for 90% CO_2 removal from flue gas (10–15 kPa CO_2) in a standard separation process usually requires stripper reboiler duties of at least 3.6–4.0 GJ per t_{CO2}. Reducing this value has become the primary goal in the chemical absorbent

research, even if the reboiler energy requirement is not the only metric that defines absorbent performance. Consequently, new absorbents are benchmarked against the value for 30 wt% MEA by default. Table 1 shows this value among the corresponding energy consumption values of other absorbents. The widespread use of MEA in industry is due to its favorable characteristics in terms of CO_2 mass transfer rate, biodegradability and cost. The most prominent downsides with this solvent are moderate levels of toxicity, moderate rates of oxidative and thermal degradation. Moreover, it has corrosive tendencies when used at higher concentrations. In the case of MEA and methyl-diethanolamine (MDEA) blends, the reboiler duty increases with higher ratios of MEA (Bui et al., 2018). Recent process development indicates that the thermal degradation and corrosiveness of MEA, when used at higher concentrations than 30 wt%, can be circumvented via additives. Introducing high performance oxidative inhibitors would enable the feasibility of 40 wt% MEA, thereby reducing the regeneration energy demand to below 3.3 GJ per t_{CO2} (Lemaire et al., 2014).

The MEA solvent is sensitive to impurities such as nitrogen dioxide (NO_2), oxygen (O_2), sulfur oxides (SO_x) and dust. The quality of the flue gases to be treated should therefore be considered when integrating a Post-CC process to an industrial process. For example, amine degradation and solvent foaming is triggered by dust and particulate matters. These impurities could also lead to plugging and scaling of process equipment. Sulfur oxides of the type SO_2 and SO_3 are formed during combustion of fuel containing sulfur and react with amines to form heat stable salts. The SO_2 concentration in flue gases from the recovery boiler and the power boiler of a pulp mill is typically lower than in the flue gas from coal-fired power plants. However, if the sulfur content would be high, the addition of a flue gas desulfurization plant should be implemented prior to the capture unit. Alternatively, the direct contact cooler (DCC) could be adjusted to scrub out sulfur components by operating with an appropriate dosage of alkali solution (IEAGHG, 2016).

Amine degradation alters the viscosity, conductivity and pH of the absorbent as well as the CO_2 absorbing capacity. Plant operation parameters affected by excessive amine-degradation rates include susceptibility of the absorbent to foam, pressure drop across packed column and the liquid to gas ratio (L/G) required to maintain CO_2 capture rates. Atmospheric emissions, amine reclamation and corrosion are some other aspects of the design and operation of a Post-CC plant that are closely related to amine degradation (Reynolds et al., 2016).

3. Swedish pulp mills

Producing pulp and paper requires large amounts of heat and power input. The pulp, paper and printing industry together stand for 5.7% of global industrial final energy use, of which printing is a very small share (IEA, 2007). The total emissions from large Swedish pulp mills, with annual emissions exceeding 500 kt, add up to around 20 Mt CO_2 per year. These emissions arise from combustion of residual biomass streams that cannot be made into pulp. The power and steam produced through combustion is primarily intended for the internal energy use in the pulp and paper mill. However, these by-product streams may in some cases undergo conversion to electricity for the purpose of external energy use (Normann et al., 2019). The following text summarizes the main processes (Figure 2) in a modern Swedish pulp mill and explains which carbon emission sources are the most relevant to consider in capture scenarios of this industry.
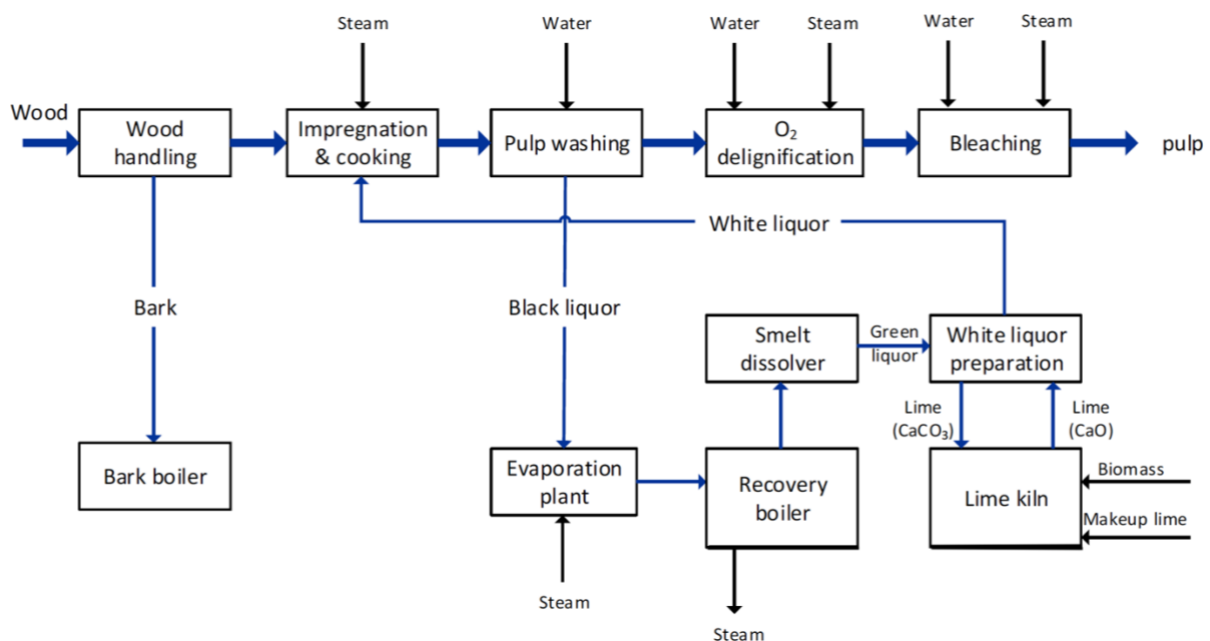
Figure 2 Overview of the key processes in a Kraft pulp mill (Normann et al., 2019)

3.1. Key processes

Chemical pulping based on the Kraft process dominates in Europe with respect to its whole production of market pulp, i.e. produced from non-integrated pulp mills. According to gathered data from 2008, Sweden was the leading pulp producer in Europe that year since all of its Kraft pulp mills combined together produced 12.1 Mt pulp per year (Suhr et al., 2015). The Kraft chemical process is also the most commonly used pulping method in Sweden. This process begins with the separation of the cellulose from the wood by cooking the raw material in a chemical mixture, the so called white liquor. While the pulp material, i.e. separated cellulose, is being processed into the desired pulp or paper product, the spent cooking chemicals will be recovered in the recovery boiler by combusting it together with the remainder of the wood, e.g. dissolved lignin. The liquid process stream entering the recovery boiler is usually referred to as black liquor (Garðarsdóttir et al., 2018). Normally, the power plant configuration in a non-integrated kraft pulp mill constitutes a recovery boiler and a power

boiler feeding a back-pressure turbine. The heat generated upon burning the strong (concentrated) black liquor in the recovery boiler is used to produce high-pressure (HP), superheated steam. Part of this HP steam will be converted to electrical power as it passes the turbine. Medium-pressure (MP) and low-pressure (LP) steam are needed to cover the heat energy demand in other parts of the kraft pulp process (Suhr et al., 2015).

Figure 3 Illustration of the main process steps of the calcium and alkali recovery circuits in a Kraft pulp mill (BMU Austria, 1995)

The recovered cooking chemicals, i.e. weak black liquor, are processed in the chemical recovery system (Figure 3) before re-used in other parts of the pulping process (ZEP & EBTP, 2012). The main processes in the chemical recovery system are black liquor evaporation, incineration of evaporated liquors and causticizing. Key functions of these process steps include:

- Recovery of inorganic pulping chemicals
- Prevention and control of pollution through significant reduction of the wastewater load discharged and extensive reduction of emissions to air
- Recovery of the energy content as process steam and electrical power
- Incineration of dissolved organic material (Suhr et al., 2015)

The black liquor collected from pulp washing usually contains around 14–18% dissolved solids and needs to be concentrated before it can be burnt. The dry solid (DS) content in the liquor is increased in a multi-effect evaporation plant to 70–85%. The upper limit for the dry solid increase is usually 72–74% at atmospheric pressure. Modern plants pressurize the liquor to concentrate it up to 85% DS. Some of the combustible material will separate as non-condensable gases (NCG) during evaporation. These gases contain malodorous gas compounds that vary in their degree of contamination according to their origin (Suhr et al., 2015). Swedish recovery boilers usually combust black liquor with a dry solid content of around 70% (FRBC, 2010). Usually, black liquor evaporation is the highest steam consumer in energy-efficient market bleached kraft pulp mills (Table 2). However, heat and electricity

consumption data should not be interpreted without specific energy balances of the mill, since methods to monitor, calculate and report the energy used differ between mills. The geographical location of the mill may also affect the heat consumption to some degree (Suhr et al., 2015).

Table 2 General steam consumption levels of a market bleached kraft pulp mill with well-designed and operated processes, expressed as an annual average. Steam for electrical power production and the primary thermal energy necessary for lime reburning are not included (Suhr et al., 2015).

Process	Cooking	O_2 delignification	Bleaching	Drying	Evaporation	Other	Total
Steam consumption (GJ/ADt)	1.6–2.0	0.2–0.4	1.5–2.0	2.2–2.6	4.0–4.5	1.5–2.0	11-12

3.1. Carbon emissions

Pulp and integrated pulp and paper mills represent the majority of the large point sources of CO_2 in this heavily industrialized region. Introducing the BECCS concept in the pulp and paper industry would therefore enable a significant potential for creating CO_2 -negative facilities in Sweden. The recovery boiler accounts for around 75% of the total plant emissions. Almost all Swedish pulp and paper mills use bio-oil rather than fossil-based oil in their lime kilns, which are responsible for 10-15% of the emissions. The remainder emissions originate from the power boiler, also around 10–15%, in which the bark and other biofuels from the wood that did not get used in the process are combusted. Because of the variable operation of the power boiler, it is considered to be the least feasible source for CO_2 capture (Garðarsdóttir et al., 2018). Besides black liquor, waste wood is sometimes also used in the recovery boiler and power boiler. These types of fuel classify as biomass derived fuels. Therefore, 75-100% of CO_2 emitted from a modern pulp mill or integrated pulp and paper mill is commonly assumed to be carbon neutral as both fuels are considered biogenic if they are sourced sustainably (Onarheim et al., 2017).

Some features of modern pulp and paper mills that have been identified as challenges in applying CCS retrofit are: technical restrictions in the plant layout, impurities in the flue gas, the size of single sources, as well as heavily integrated processes (ZEP & EBTP, 2012). Energy supply can also be a limiting factor for carbon capture implementation when paper production is integrated in Kraft pulp mills (Kuparinen et al., 2019). Thermal integration of the capture process is usually considered with the intention of improving energy efficiency upon implementation of carbon capture at different mills. Most importantly, it is the plant-specific process layout that reflects on the potential for such integration. True steam surplus is commonly available at Kraft pulp mills and pure thermomechanical pulp mills. On the other hand, integrated Kraft pulp and paper mills and paper mills without virgin pulp production lack steam surplus and would therefore need to import external fuel to cover the extra heat demand that the capture process implies (Jönsson & Berntsson, 2012). New opportunities for BECCS may emerge if black liquor gasification is introduced or when the Swedish pulp and paper industry start including biofuels and/or specialty chemical production, i.e. biorefining (Rootzén et al., 2018), in their product and process portfolios.

3.2. Process integration

System solutions are as important as new technologies for reducing energy use in industry. Process integration measures vary from case to case in terms of technical solutions and energy saving. Identifying where and to what extent process integrations tools have been used and how much they have contributed to energy saving is more difficult than with new technology solutions. The three main features of process integration methods are the use of: rules of thumb (heuristics), thermodynamics and optimization techniques. There is usually a significant overlap between various methods. Nowadays, the trend is strongly towards methods that incorporate all three features. Exergy analysis and pinch analysis are methods with particular focus on thermodynamics. The latter has proven to be powerful when developing new mill processes and concepts. Large potentials for energy savings in the pulp and paper industry have been identified through studies in the United States, Canada, Finland and Sweden. Results from these process integration studies, mainly pinch analyses, have been implemented in more than 100 mills worldwide. New process integration tools and methods, e.g. more efficient heat exchanger networks, can lead to energy savings in the order of 10–40% for chemical pulp mills with relatively high energy consumption. Novel system solutions, such as integration of the secondary heat system and the evaporation plant, can lead to energy saving in the order of 15-30% for energy efficient mills (IEA, 2007).

Even though the emission levels from the pulp and paper industry are comparable to those of fossil-fueled industries, no pilot or demonstration initiatives focusing on CCS have been established for this industry yet (Garðarsdóttir, 2017). Instead, several conceptual studies have been conducted in order to assess the viability of implementing BECCS in the pulp and paper industry. Onarheim et al. (2017) concluded in one of these studies that favorable opportunities for heat integration may exist for this industry by implementing CO_2 capture technologies. Their evaluation considered two hypothetical reference mills situated in Finland and the capture cases assessed involved the CO_2 emissions of the flue gases from the recovery boiler, the power boiler and the lime kiln and various combinations of these. The results indicated that the technical feasibility of retrofitting Post-CC to an existing pulp mill or pulp and board mill is very dependent on the existing power and steam production onsite. For example, in the case of an integrated pulp and board mill that aims for 90% capture rate, excess steam produced onsite will not be sufficient and will therefore require an auxiliary boiler to assist with supplement steam. Whether the extra steam demand of the CO_2 capture plant is sufficient or not also depends on the flue gas volume and its partial pressure of CO_2.

4. MEA process modelling

This chapter begins with the description of a process flow diagram consisting of two major parts, the absorption and desorption processes. The absorber is the most expensive and largest unit (Øi, 2010), whereas the reboiler connected to the desorption column is the main contributor to the total energy demand of this capture process (Li et al., 2016). Then, a brief comparison between equilibrium-based and rate-based models will be provided prior to explaining the most relevant chemical reactions in the MEA process.

4.1. Standard process configuration

A schematic representation of the amine-based Post-CC plant is given in Figure 4. The flue gas will enter the bottom the absorber (2) after passing through the flue gas conditioning unit (1) that usually includes a DCC, where it is quenched and most of the residual particular matter is removed (IEAGHG, 2016). The absorber operates at a lower temperature than the stripper to ensure a higher affinity for CO_2 absorption. The lean amine solvent will selectively absorb CO_2 as it comes in contact with the flue gas throughout the absorber packing. CO_2 dissolves into the absorbent after it has diffused from the bulk gas to the gas-liquid interface. As CO_2 reacts with the amine present in solution, its concentration will be depleted at the gas-liquid interface. This decrease is what maintains the driving force for CO_2 to move from the gas to the liquid phase (Puxty & Maeder, 2016). While the solvent flows downwards through the absorber, the CO_2-lean gas moves countercurrent with it and passes through the washing section at the top of the column before it is emitted to the atmosphere. Any traces of amine components and degraded by-products will be removed from the treated flue gas in the water wash section, in the top part of the absorber column (Onarheim et al., 2017).
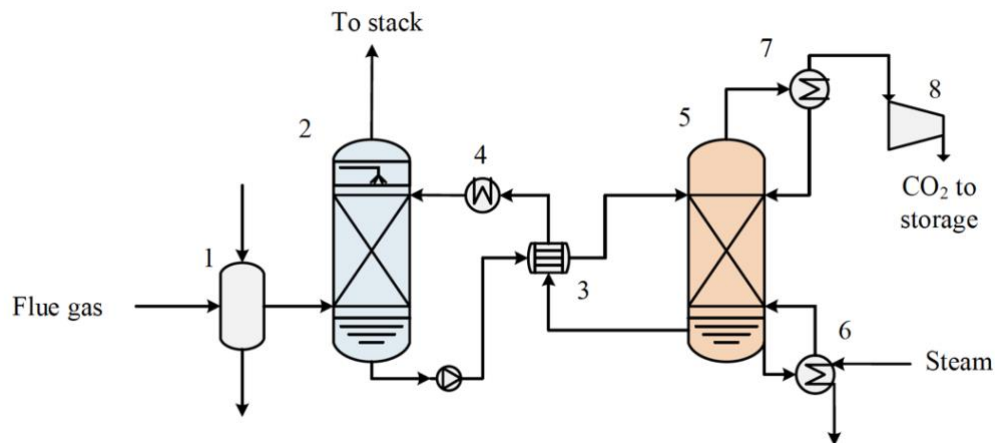
Figure 4 Conventional CO_2 absorption-desorption process configuration (Garðarsdóttir, 2017).

The CO_2-rich solvent is withdrawn from the bottom of the absorber and is then directed to the top of the stripper (5) through the solvent heat exchanger (3), in which residual heat from the hot CO_2-lean solvent is recovered. Hot steam is produced in the stripper reboiler (6) and flows upwards counter-currently to the rich solvent to assist in the thermal regeneration of the absorbent. Steam is used in the desorption column to maintain the absorbents temperature since the process is endothermic, as well as to maintain the desorption driving force by diluting the CO_2 being released below the equilibrium partial pressure (Puxty & Maeder,

2016). The regenerated solvent discharged from the bottom of the stripper is cooled in two steps before re-circulating it to the top of the absorber column. First, it is pre-cooled in the solvent heat-exchanger (3) and then in the solvent cooler (4) where water is used as cooling medium. The wet CO_2-rich gas exiting the stripper will pass through a condenser (7) for moisture removal before sending it to the CO_2 compression train (8) (Onarheim et al., 2017).

4.2.   Equilibrium and rate-based models

The historical approach to simulate separation columns has for long been based on the equilibrium-stage concept, in which the vapor and liquid phases are assumed to be at a state of thermodynamic and chemical equilibrium at each theoretical stage. Although, streams leaving a real tray or section of a packed column are not in equilibrium. The actual separation achieved in real columns depends on the rates of mass transfer from the vapor to the liquid phase. The magnitude of these rates in turn depends on the extent to which the vapor and liquid streams are not in equilibrium with each other. Furthermore, neither reaction kinetics or film diffusion are considered within this approach, causing inconsistency in simulation results for chemical absorption and desorption processes. The rate-based model should therefore be used in reactive systems (Taylor et al., 2003) as it considers the material transfer and the kinetics of the chemical reactions present along the column packing while the equilibrium is only assumed to occur at the gas-liquid interface (Neveux et al., 2017).

As flow scheme modifications shift the kinetics and thermodynamics in columns, the use of equilibrium stages in such studies is particularly suboptimal. For example, the addition of an intercooler in the absorber will in theory enhance the solubility of CO_2, thus maximizing the driving force for absorption, but at the cost of a lower reaction rate which in turn minimizes the transfer rate. Such a modification entails withdrawal of the solvent passing at an intermediate point in the column and cooling it down before it is sent back into the absorber. Now, when adding an intercooler to an absorption process using 30 wt% MEA as solvent, an equilibrium-stage model predicts around 12% reduction of the reboiler heat duty (Ahn et al., 2013), while both pilot plant experiments (Knudsen et al., 2011) and rate-based simulations (Le Moullec & Kanniche, 2011) with the same process modification demonstrate a much lower reduction (1 to 2%). Consequently, rate-based models should be regarded as mandatory for accurate predictions in process design studies (Neveux et al., 2017).

The simulation results of Zhang and Chen (2013) from the equilibrium model of a stripper indicate a clear tendency toward underestimation of the reboiler heat duty when compared to experimental data and simulations results from a rate-based approach. Moreover, the same equilibrium-stage model in their study overpredicted the CO_2 removal percentage and provided poor predictions of the temperature and CO_2 concentration profiles in the absorber. A way to produce similar results as those from a rate-based approach is by tuning the Murphree efficiency values with a trial and error technique until the simulation results show a closer agreement to experimental data (Marik Singh et al., 2017).

Considering that the main energy consumer is the reboiler, the use of either a rate-based method or an equilibrium setup for the desorption column adjusted to match results of a rate-based one should be emphasized when economical aspects will be part of the optimization analysis in a steady-state design. There are cases though, in where the equilibrium approach is preferred, such as when other data systems (e.g. electricity, weather and carbon markets) are to be incorporated in dynamic data-driven models (Abdul

Manaf et al., 2016) and upon evaluation of the dynamic performance of different scenarios expected to occur during operation (Aspen Technology, Inc., 2014) or in emergency situations (Øi, 2010).

4.3. Modelling tools

The evaluation of process performance of various plant configurations by building and operating infrastructure can be costly. Using simulation software is a much less costly approach to assess process plant performance, in regard to time and capital (Bui et al., 2014). Therefore, computer-aided process simulation is nowadays recognized as an essential tool in the chemical process industries. It plays a key role in the evaluation of technical and feasibility studies, investigation of feed flexibility, flow-sheet optimization and interpretation of pilot plant data. A lot of mathematical models are usually involved when performing process simulation calculations. They can be thermodynamic, non-equilibrium, physical property or fluid mechanics models (Solbraa, 2002). Commercially available software that have been used to model amine-based Post-CC processes at steady-state conditions are: Aspen HYSIS, Aspen Plus, Pro/II and ProMax (Øi, 2010). Moreover, the absorption part of the capture process has been simulated dynamically, i.e. the system changes over time, using Matlab (Conference on Mathematical Modelling & Troch, 2009) and gPROMS (Kvamsdal et al., 2009).

Each of these process modelling tools have their own strengths, weaknesses and special features. For example, both Aspen HYSIS and Aspen Plus use a sequential modular flow-sheeting framework by default. This extremely effective and commonly used approach works with an algorithm that allows the simulation to go in one direction only: downstream. In the case of Aspen Plus, where the modules can only be executed one at a time, the algorithm will consider the order in which they should be computed as it analyzes the flowsheet by following the flow of material, energy or information. The output streams and other performance information of each block will only be calculated when all the input streams details and necessary model parameters have been specified. In contrast, HYSIS has an inbuilt ability for information to move upstream as it allows for the user to specify a desired outlet stream temperature into the form for the outlet stream rather than into the form of the heat exchanger. Entering user information into the stream would be ignored in Aspen Plus.

The rate-based model makes use of correlations to predict the actual performance of small packing sections and does not involve height equivalent of a theoretical plate. Instead, the attainment of equilibrium is assumed to occur at the gas liquid interface only (Solbraa, 2002). The RadFrac model in Aspen Plus uses rigorous inside-out algorithms by default to solve a system of nonlinear algebraic equations consisting of phase equilibrium, energy balance, material balance and summation equations for each theoretical stage. These algorithms consist of two nested iteration loops. An approximate set of thermodynamic parameters are used in the inner loop to solve the system of equations. Exact thermodynamic models are employed in the outer loop to update the parameters of empirical equations used in the inner loop (Haydary, 2018).

HYSIS will automatically compute information for some blocks by default without having to run the full simulation as soon as enough data are available. On the other hand, Aspen Plus has the advantage of automatically selecting tear streams based on flow-sheet structure. This

is an attractive feature to some users as it relieves you from the habit of always having to think about adding a Recycle block whenever the solver needs an abstract point to generate new guesses at each iteration, which is the case for HYSIS and ProMax. Pro/II is similar to Aspen Plus in this aspect, as well as when it comes to their general form-based model construction and sequential modular flowsheets. Although some of their libraries of chemicals and physical property models are different from each other, both tools are suitable for integration with other software for the purposes of process control, optimization and dynamic modelling.

ProMax on the other hand, besides being similar to HYSIS in functionality, is a software specifically created for CO_2 removal and gas sweeting applications and therefore includes optimized proprietary convergence algorithms for absorber and stripper models. Another practical feature is that it exists as an add-on module to Microsoft Visio. Besides being a chemical process tool, gProms is also an advanced ordinary differential equation integrator that operates in an equation-oriented environment. The model created in the graphical user interphase of this software can be either steady-state or dynamic and will ultimately consist of one large system of equations. It is also possible to build the models from scratch using custom equations. Aspen Plus has a significant advantage over gProms for steady-state simulations when operating in equation-oriented mode since the sequential modular mode can be used to initialize and solve the flowsheet with less degree of difficulty (Adams, 2018).

4.4. Thermodynamics and kinetics

The electrolyte-non-random-two-liquid-based thermodynamic package "ENRTL-RK" was selected to describe the thermodynamics in the MEA process since it considers the strong non-ideality of the liquid electrolyte solution. The coupling with the Redlich-Kwong (RK) equation of state in this model enables the computation of the vapor properties (Madeddu et al., 2019). The chemistry of the MEA- CO_2 - H_2O system can be represented by a set of equilibrium and reversible kinetic reactions. The reactions shown in Table 3 are widely used for modelling purposes, including by (Freguia & Rochelle, 2003), and will therefore also be used in this study.

Table 3 Chemical reactions considered in the MEA process.

No.	Type	Reaction
1	Equilibrium	$2H_2O \rightleftharpoons H_3O^+ + OH^-$
2	Equilibrium	$MEAH^+ + H_2O \rightleftharpoons MEA + H_3O^+$
3	Equilibrium	$HCO_3^- + H_2O \rightleftharpoons H_3O^+ + CO_3^{2-}$
4	Kinetic	$MEA + CO_2 + H_2O \rightarrow MEACOO^- + H_3O^+$
5	Kinetic	$MEACOO^- + H_3O^+ \rightarrow MEA + CO_2 + H_2O$
6	Kinetic	$CO_2 + OH^- \rightarrow HCO_3^-$
7	Kinetic	$HCO_3^- \rightarrow CO_2 + OH^-$

Reaction 1 is the water dissociation, reaction 2 the protonation of MEA and reaction 3 the bicarbonate dissociation. Reactions 4 and 5 are the forward and reverse reactions for carbamate formation, and reaction 6 and 7 are the forward and reverse reactions for bicarbonate formation. The necessary parameters for the calculation of the chemical equilibrium constants for reactions 1–7, using the standard Gibbs free energy change, were

obtained from the databank of Aspen Plus. Power law expressions (Eq. 1) were used to calculate the reaction rates, *r*, of reactions 4–7.

$$r = kT^n exp\left(\frac{-E}{RT}\right) \prod_{i=1}^{N}(\chi_i \gamma_i)^{a_i}$$ (1)

In order for the simulation to proceed one needs to provide the software with the activity basis rate constants, *k* and *E*, of each forward and reverse reaction considered in the thermodynamic model. The pre-exponential factor *k* and the activation energy *E* are tabulated in Appendix A – Absorption validation: parameters and results. *T* is the absolute temperature, *R* is the universal gas constant, *N* is the number of components in the reaction, χ_i is the mole fraction of component *i*, γ_i is the activity coefficient of component *i* and a_i is the stochiometric coefficient of component *i* (Aspen Technology, Inc., 2014). In this study, the factor *n* is zero.

4.5. Material transport

Three main theories have been suggested for the quantification of the material transport across the gas-liquid interface in the rate-based model: the two-film theory by Lewis and Whitman, the penetration theory by Higbie and the surface renewal model by Danckwerts. The most used theory for CO_2 absorption is the two-film theory since a significant number of correlations for the parameters evaluation are easily accessible in literature. In this theory, all the resistance to material and energy transfer is assumed to take place in two thin films close to the gas-liquid interface. As showed in Figure 5, the spatial domain represented by the rate-based segment can be divided in four parts: gas bulk, gas film, liquid film and liquid bulk. The absorption process involves the mass transfer of CO_2 from the gas bulk to the interface, through the gas film, followed by absorption into the liquid where it will react with the solvent. Reactive columns in the RadFrac model are considered as a finite number of continuous stirred-tank reactors (CSTRs) connected in series. Five different flow models are available in the RadFrac model for evaluation of the bulk conditions in each segment: mixed flow (bulk properties=outlet conditions which approximates an ideal CSTR), countercurrent flow (bulk properties=average between the inlet and the outlet conditions), and VPlug/VPlugP/LPlug flow (average conditions for one phase and outlet conditions for the other one) (Massimiliano et al., 2019).
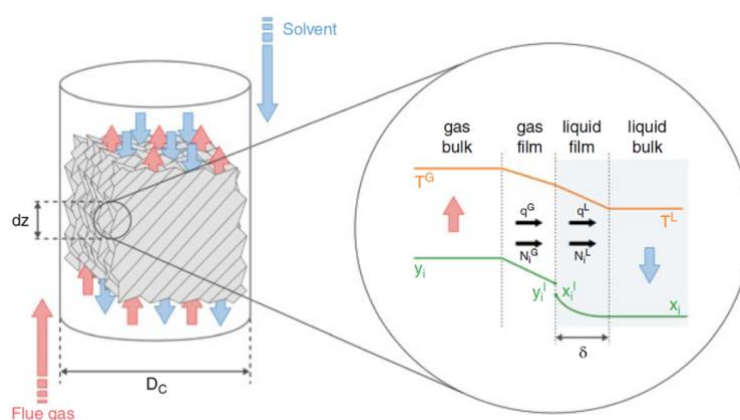
Figure 5 Heat (q), and mass (N) transfer fluxes on a differential element of packing, dz. In this schematic representation of the two-film theory, the mole fractions in the gas and liquid phases are x and y, respectively. T denotes the temperatures (Neveux et al., 2017).

5. Methodology

In the validation of the absorber, the focus was on the liquid temperature profile, CO_2 removal efficiency and the rich loading (i.e. CO_2 loading in the rich solvent at the absorber outlet). Next, the amount of amine solvent and the diameter and packing height of the absorber (5.3.1. Absorber) and stripper (5.3.2. Stripper) are determined in order to satisfy the intended performance of the capture plant according to the design criteria as presented in the next section (Table 8). The sizing of the absorber and stripper also took into consideration the characteristic composition, flowrate, temperature and pressure of a flue gas stream originating from the recovery boiler of a stand-alone softwood market pulp mill. The existing low-pressure (LP) steam at 4.5 bar may be extracted from the steam cycle to provide the required steam in the stripper reboiler (Normann et al., 2019). A schematic of the workflow is shown in Figure 6.

Validation

- absorber (lab and pilot scale)
- stripper (two different reflux configurations)
- adjustments in Property environment
- adjustments in Simulation environment

Setting up standard process

- connection between absorber and stripper
- figuring out tear streams
- reconstruction of stripper reflux

Sizing

- discretization (no. stages)
- solvent flow rate
- 90% capture rate
- pressure drop ($\triangle P$)

Stripper modification

- adding a compressor before condenser
- varied operation pressure (1, 1.3 and 1.8 bar)
- heat curves from condenser evaluated for different compressor discharge pressures (4-10 bar)

Figure 6 Workflow of the modelling and simulation steps needed to reach the thesis objectives.

The CO_2 loading gives an indication of the absorption capacity of the solvent (Madeddu et al., 2018) and is defined as the ratio between the CO_2 and MEA apparent molar fractions according to Eq. (2). This performance indicator was calculated for every simulation in Aspen Plus by creating the Property Set, ML-LOAD, in the Properties Environment and then adding it to the report page through two steps in the Simulation Environment: first by selecting the corresponding ID in the Property Sets window from the Setup | Report options | Stream tab and then selecting it again in the Analysis | Report | Properties tab of each RadFrac block.

$$Loading = \frac{x_{CO_2}^{app}}{x_{MEA}^{app}} = \frac{x_{CO_2} + x_{HCO_3^-} + x_{CO_3^{2-}} + x_{MEACOO^-}}{x_{MEA} + x_{MEAH^+} + x_{MEACOO^-}} \tag{2}$$

5.1. Validation

The model used in this study was validated by following the main steps of a systematic procedure developed by Madeddu et al. (2019). One of the most highlighted steps in their validation process is the evaluation of number of segments, i.e. discretization points in axial direction of the packing section. The main reason for such analysis being that a sufficiently high number of segments is needed from a mathematical point of view to obtain a correct numerical solution of the process model. The appropriate number of segments is identified by varying this parameter until the difference between two consecutive sets of profiles, e.g. temperature profile, becomes negligible. Another positive effect of the special consideration to the discretization of the axial domain is the fact that the temperature bulge also gets correctly described. For example, it takes 30 segments for the temperature bulge to start showing in the computed temperature profile of the lab-scale absorber.

The appropriate amount of discretization points depends from case to case. Usually, the larger the column the greater the number of segments is needed to correctly describe the absorption/desorption process with the RadFrac model in Aspen Plus. The adequate number of segments was evaluated for all absorption/desorption cases studied in this work.

5.1.1. Absorber

The absorption model was validated by comparing model predictions and literature data. The literature data are taken from two pilot-plant facilities that differ in operating conditions, size and packing type (random vs. structured): a lab-scale and a large-scale absorption plant. Experimental data from only one run from each plant was selected for the model validation: T22 (Tontiwachwuthikul et al., 1992) from the lab-scale and 1-A2 (Razi et al., 2013) from the pilot-scale plant. After setting up the Properties and Simulation environment in Aspen Plus some other values needed to be provided to enable the simulation run: the kinetics parameters for the reversible reactions (4–7 in Table 3) and the Henry's law constant coefficients for CO_2-H_2O and CO_2-MEA. The Henry's law constant is an important solvent property parameter to consider in the absorption process as it represents the solubility of CO_2 in a given solvent (Bui et al., 2018).

Neither of these input parameters were provided by the Aspen Plus databank by default upon choosing the ENRTL-RK thermodynamic package for the MEA-CO_2-H_2O system. These values therefore had to be found in literature. Six different sets of kinetic parameters were tested and only two of these resulted in adequate fitting with experimental data when combined with a suitable set of Henry's law constant coefficients. However, the simulation results were still not matching those from the experimental data (see case D0 for the pilot-scale absorber in Table 4) which is why different combinations of electrolyte pair parameters (GMENCC) were evaluated together with the most promising sets of kinetic parameters. These parameters relate to molecule-ion and ion-ion interactions in electrolyte solutions and are also required for the calculation of major thermodynamic properties when using the ENRTL-RK method. To keep better track of these changes, the combined kinetic and GMENCC parameters were referred to as G0–G4 and D0–D4. See Appendix A – Absorption validation: parameters and results for more details about the results presented and to better understand the notations used in this section.

Table 4 Comparison of experimental data with simulation results of performance indicators of some of the absorption cases tested in the validation procedure.

	Performance	D0	D1	D3	Experimental
Pilot-scale	CO_2 removal (%)	66.2	63.6	89.5	90
	Rich loading	0.436	0.427	0.510	-
Lab-scale	CO_2 removal (%)	98.2	94.8	98.1	100
	Rich loading	0.461	0.450	0.461	0.443

While the same set of chemical reactions is used to model both the absorber and stripper in most cases, some studies have proposed different reaction kinetics in regard to reaction 5 (Table 3), which dictates the rate of CO_2 desorption. In that case, the reaction rate constants are calculated through linear regression (Aspen Technology, Inc., 2014). Depending on the chosen temperature range for the absorber and stripper respectively, the output values will differ. This and other measures to adjust the kinetic parameters depending on the operation conditions of the process could explain why the values found in literature differed so much from each other.

According to (Kvamsdal & Rochelle, 2008), the liquid-to-gas mass ratio (L/G) is one of the main factors that influence the location and magnitude of a bulge in a temperature profile. The bulge is usually located at the column top for values of L/G lower than 5, while for values of L/G above 6 it is located at the bottom part. The needed L/G value to reach the required separation performance is usually low in columns filled with structured packing, mainly because of their higher surface area compared to random packed columns. Consequently, bottom bulges are typical in random packed columns (Errico et al., 2016). Figure 7 shows the temperature profiles of the absorption columns calculated with the different model cases presented in Table 4. The model consistently predicts a temperature bulge in the top section of the column for the pilot plant. This is expected because of a 4.1 value for the L/G in this example. On the other hand, a bottom temperature bulge shows in the temperature profile of the lab-scale plant, which is no surprise considering its relatively high L/G value of 7.43.
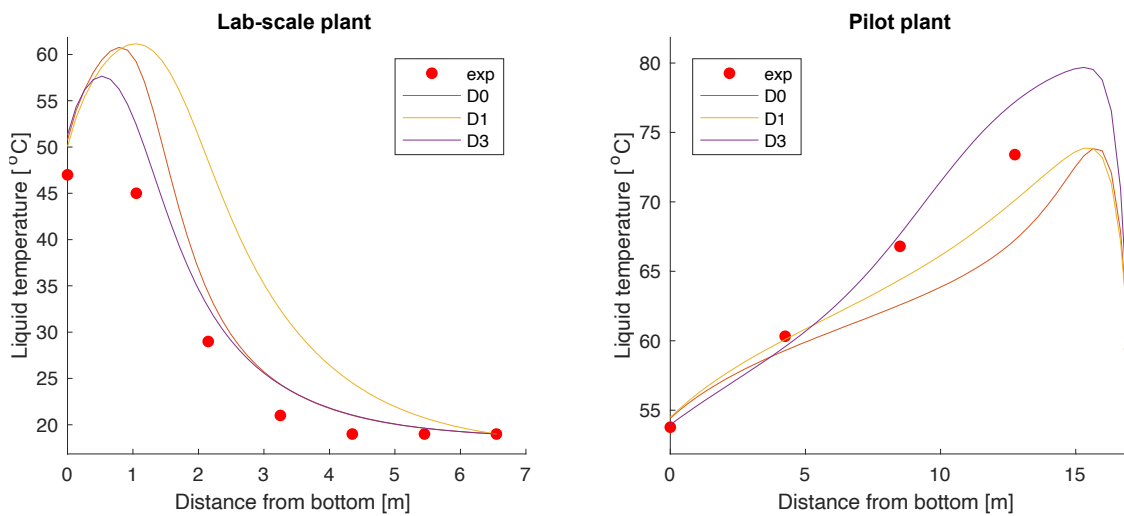
Figure 7 Temperature profiles of the absorber columns in the lab-scale and pilot plant, calculated with 50 stages with different combinations of electrolyte pair parameters. Experimental data (exp) relates to different points throughout each packing section.

The results from the D3 alternative excelled in similarity with the literature values in regard to the absorber performance: with no more than 2% error in the estimation of the CO_2 removal efficiency and 4% error in the estimation of the rich loading (Table 4). The good agreement between the model and experimental results (independently of the operating conditions, the column dimensions and the temperature bulge location) indicates that alternative D3 can be used with confidence when conducting a new absorber design.

5.1.2. Stripper

The desorption model was validated by comparing model predictions and literature data. The literature data for this validation step are taken from two pilot-plant facilities that differ in operating conditions, size and packing type (Sulzer Mellapak 250Y vs. Flexipac 1Y). These were, the pilot plant facility of SINTEF (a Norwegian independent research organization) and the pilot plant facility of University of Texas at Austin (UTA). Experimental data from only one run from each plant was selected for the model validation: no. 1 (Tobiesen et al., 2008) from the SINTEF plant and no. 47 (Dugas, 2006) from the UTA plant. The stripping section in both of the plants is equipped with structured packing, a reboiler and a partial condenser. The main difference between the two cases is in how the water stream exiting the condenser is distributed to other parts of the stripper. In the SINTEF case, the condensed water is mixed with the lean solvent exiting the stripper bottom before entering the reboiler. The UTA case, on the other hand, resembles the desorber configuration of a standard MEA process since the condensed water is sent back to the stripper top as reflux. Also, the run that was selected from the UTA plant operated under vacuum condition (0.69 bar) and that from the SINTEF plant at higher pressure (1.96 bar).

Table 5 Error in the estimation of the reboiler duty with number of segments for the UTA plant.

Model	Performance	Number of segments			Experimental
		10	80	90	
I	Reboiler duty (kW_{th})	292	251	250	205
	Error (%)	43	22	22	-
II	Reboiler duty (kW_{th})	249	217	217	205
	Error (%)	21	6	6	-

To prove validity of the MEA model in the case different experimental data sets are available, Madeddu et al. (2019) chose the degrees of freedom differently for each plant. The same concept was also applied in this study. The UTA stripper was the first one validated, in which the condenser temperature and the CO_2 gas molar flow rate (hence, also the lean loading) were fixed by assigning two design specifications inside the RadFrac block. Using the same model correlations as the ones used during the absorber validation (Model I) gave a 22% error upon estimation of the reboiler duty, see Table 5. Instead of tweaking parameters in the Properties environment, as was the case in the absorber validation, it was decided to adjust other parameters directly in the Simulation environment through the sheets in Rate-Based Modeling | Rate-based Setup. Model II resulted from this adjustment of parameters.

The parameters that differ between the two models are: reaction condition factor, interfacial area method, interfacial area factor, heat transfer factor, liquid mass transfer coefficient factor and vapor mass transfer coefficient factor. See Appendix B – Stripper validation: parameters

and results for detailed parameter specification of the models. The temperature in the stripper column in both examples was overestimated, although quite consistently, with 1–2ºC for the UTA plant and 2–3ºC for the SINTEF plant (Figure 8). The overestimation of the temperatures still remains when using model II.
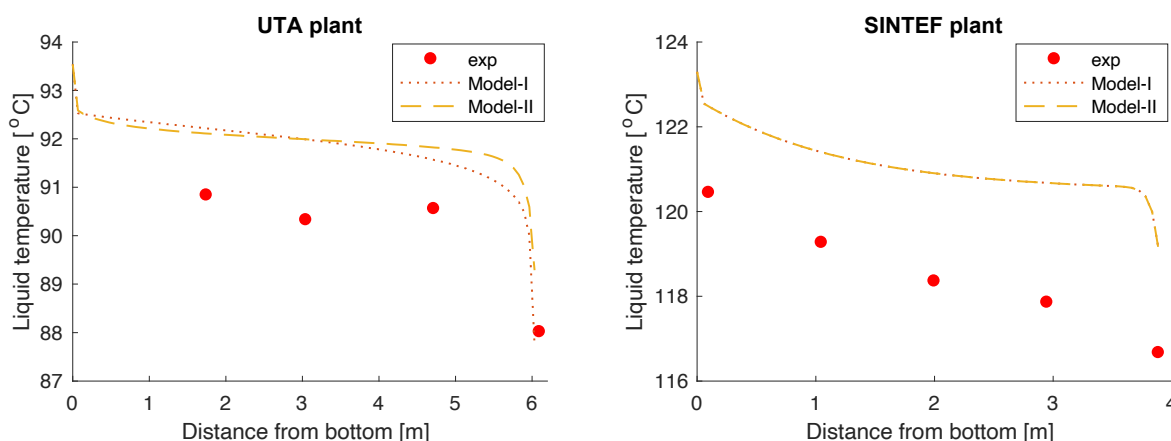
Figure 8 Temperature profiles of the stripper columns for the UTA and SINTEF plant calculated with 90 stages. The simulation results include the reboiler temperature (bottom). Experimental data (exp) relates to different points throughout each packing section.

Differently from the validation of the UTA plant, the condenser temperature and the reboiler duty were fixed in the simulation of the SINTEF plant. Consequently, the performance value evaluated in this example was the lean loading, i.e. CO_2 loading in the lean solvent stream exiting from the bottom stage. Similar to the overprediction of the reboiler duty, the loading was also overpredicted in the stripper validation of the SINTEF example. Although, it was not possible to reduce the error in the estimation of this performance value, by changing from Model I to II, to the same extent as with the UTA stripper. The suggested model overpredicted the lean loading from the SINTEF stripper with 14% (see Appendix B – Stripper validation: parameters and results).

5.2. RadFrac model

The Aspen Plus RadFrac distillation column, based on the two-film theory with a rate-based approach, was used as a basis for simulating the absorber and stripper units in this work. This method is by far one of the most popular choice among researchers for simulation of MEA-based CO_2 capture processes (Biermann et al., 2018; Errico et al., 2016; Ferrara et al., 2017; Fosbøl et al., 2014; Freguia & Rochelle, 2003, p. 2; Garcia et al., 2017; Garðarsdóttir et al., 2018; Hasan et al., 2012; Hwang et al., 2019; Le Moullec & Kanniche, 2011; Li et al., 2016; Luo & Wang, 2017; Madeddu et al., 2018; Marik Singh et al., 2017; Onarheim et al., 2017; Razi et al., 2013; Zhang & Chen, 2013). Transport property models are necessary for the determination of various physical and thermal properties such as viscosity, density, surface tension, thermal conductivity and diffusivity. These models are based on empirical correlations involving flow parameters and fluid properties such as heat and mass transfer coefficients, interfacial area, pressure drop and liquid holdup (Hasan et al., 2012). Table 6 summarizes the correlation parameters used to model the absorption and desorption columns.

Table 6 Selected correlation parameters for the RadFrac model.

Model and column properties	
Packing material	Sulzer Mellapak 250Y
Flow model	Mixed
Film resistance	Discretize film for liquid Consider film for vapor
Discretization points for liquid film	5
Mass transfer correlation method	(Bravo et al., 1985)
Heat transfer correlation method	Chilton and Colburn
Liquid holdup correlation method	(Bravo et al., 1992)

The mixed flow model was chosen over e.g. countercurrent (which in theory should predict more accurate results for packing) because of convergence difficulties in this study with the latter option. (Zhang et al., 2009) evaluated how well the different flow models in RadFrac predict CO_2 loading, CO_2 removal% and temperature profiles of a pilot plant absorber. They concluded that the different flow models have only very minor influence on the overall capture rate performance, and that the mixed flow model predicted the most reliable predictions in regard to the temperature profiles. To ease convergence in the absorber block even more, the number of maximum iterations was increased to 100 and the damping level was set to Mild on the Convergence| Convergence | Basic sheet. The number of maximum iterations was also increased to 100 in the stripper block. Although, since the absorber block was more difficult to converge than the stripper block, a specific convergence algorithm was selected by choosing Absorber=Yes on the Convergence| Convergence | Advanced sheet. This alteration of the standard algorithm for simulation of the RadFrac model could not be selected for the stripper blocks in this work since they had an inbuilt reboiler.

5.3. Dimensioning

The flue gas characteristics (Table 7) considered in this study originate from simulation calculations of a reference pulp mill model developed by RISE Bioeconomy in WinGEMS (a simulation tool that is primarily used for mass and energy balances in the pulp and paper industry). This mill has a design capacity of 700 000 air dry tonne (ADt) of pulp per year. The recovery boiler, lime kiln and power boiler are responsible for the major CO_2 emissions from this plant. However, only the flue gas from the recovery boiler is considered for the carbon capture in this study.

Table 7 Flow rate, temperature and composition of the wet flue gas from the recovery boiler in the reference pulp mill.

Flue gas rate (tonne/h)	722
Temperature (ºC)	175
CO_2 (wt%)	20.8
N_2 (wt%)	63
O_2 (wt%)	2.4
H_2O (wt%)	13.8

The generated steam for the pulping process originates from the combustion of the remaining bark (after the refining process) in the power boiler (Normann et al., 2019). It is also assumed

that SO_2 and other impurities in the treated flue gas stream have already been removed by optimization of the process conditions during combustion and through other flue gas cleaning processes than those included in the CO_2 capture plant (Skagestad et al., 2018).

To avoid underestimation of the column dimensions and required duty, the packing section was modelled with 100 stages in the absorber and with 70 stages in the stripper. Since the stripper is equipped with a reboiler and a condenser, the packed section in this column constitutes of 68 discretization points. A column flooding limit had to bet set to determine the absorber and stripper diameters with reference to a specific point in each column. This value was fixed at 80% and the base stage was chosen to represent the more stressed (limiting) part of the column. The base stage was identified as the column stage that had the highest vapor flow rate by looking at the column hydraulic results after each simulation run.

An approximate value for the limiting stage could easily be found in the Column Internals | INT-1 | Column Hydraulic Results report of each RadFrac block. Although, the value was only true with ±1 precision upon comparison with the more precise number depicted in the column hydraulic results. The base stage and flooding limit were input values in the Design tab. The design-mode option in this tab had to be activated to enable calculation of the optimal column diameter. The following steps in the design analysis consider each absorption/desorption column as standalone, hence, the simulation results obtained from section 5.3.1. Absorber are later used as initial guesses in section 5.3.2. Stripper. Following this coupled system analysis (Madeddu et al., 2018), it was decided to introduce another constraint: that the packing height/diameter ratio of both the absorber and stripper must be higher or equal to 1. The pressure drop was considered by using a correlation from literature: 20.83 mmH_2O per meter of packing (Luo & Wang, 2017).

5.3.1. Absorber

The motivation behind testing different solvent flow rates was to avoid the presence of isothermal zones in the column (plateau shape). Thereby, ensuring the use of the entire packing. The height of each example (Figure 9) corresponds to the minimum required for 90% capture rate and was decided through design specs followed with the sensitivity analysis block in Aspen plus. The design specs block was used to fix the constraint that not more or less than 10 wt% of CO_2 leaves with the exiting gas stream, and through that obtain an approximate value of the minimum lean solvent flow rate (L_{min}). L_{min} is a term defined in the infinite method as the required solvent rate through a theoretical column of infinite height (taken here as 100 m) which was modelled with 100 segments in this study.

The sensitivity analysis comprised the computation of the mass flow rate of the CO_2 in the exit gas stream of the absorber together with the corresponding lean solvent flow rate. Since the results from the sensitivity analysis were more accurate than those from the design specs, the former was used to select a suitable L_{min} (2190 tonne/hr). The minimum numbers of absorbers were also determined through this first step of the column dimensioning process. According to different works in the literature (Madeddu et al., 2019), the diameter of absorbers with this type of packing should not be higher than 12 m. Since it was found that the absorber diameter to process the recovery boiler flue gas is ca 10.7 m (Appendix C – Absorber dimensioning for more details), the design analysis continued with the conclusion that only one absorber unit is needed to meet the capture criteria in this study.
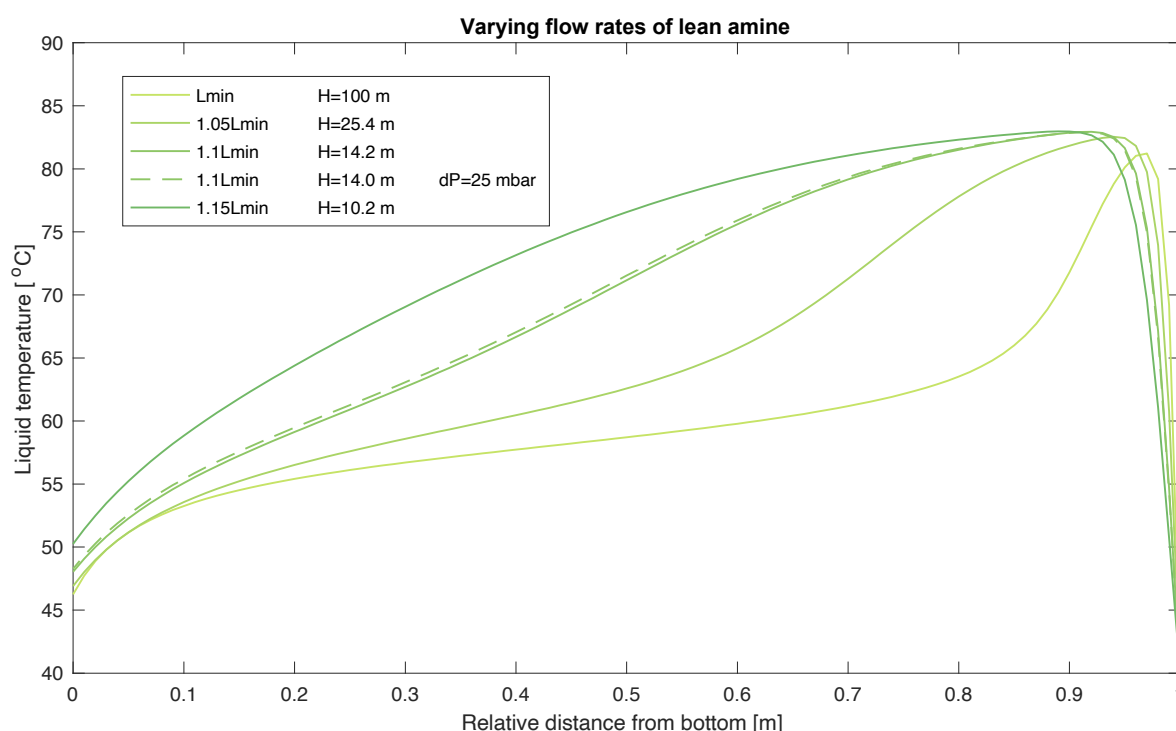
Figure 9 Varying flow rates of the MEA solvent with 0.25 lean loading that enters the top of the absorber column. L/G ratios increased from 3.4 to 3.9 when increasing Lmin to 1.15Lmin.

As shown in Figure 9, the higher the solvent flow rate the shorter column height is needed to remove a fixed amount of carbon dioxide. The dashed line represents the simulation results from when the absorber was modelled with pressure drop. The temperature profile with 1.15Lmin is also plotted there. However, the corresponding column height (10.2 m) with these conditions is lower than the column diameter, thus violating one of the main design criteria, i.e. H/D ratio should not be less than 1. It was therefore not suitable to choose these dimensions. It was decided to have an absorber equipped with a 14 m packed structured column with 11 m in diameter, thus a lean solvent flow rate of 2410 tonne/hr (=1.1L_{min}), since the temperature profile achieved with these process parameters does not indicate any plateau shape and efficient use of the entire packing will be ensured (theoretically).

The higher the column height the higher the capital expenses of the capture plant, which is why one aims to choose the column height to be as short as possible. A pressure drop was added to the absorber model and its resulting temperature profile is represented with a dashed line in the figure above. The temperature point maximum is located on the absorber top, which is typical in absorbers with structured packings with L/G values lower than 5. The L/G ratio achieved with this absorber size is 3.7 which means that the temperature profile produced with this Aspen Plus aligns with literature inferences regarding this aspect.

5.3.2. Stripper

Appropriate dimensions of the stripper column were obtained by having the starting values of the rich solvent with regard to flow rate, temperature, pressure and composition be almost the same as the output values generated in 5.3.1. Absorber. The pressure and temperature of the rich solvent were significantly altered (compared absorber outlet values) since the solvent was passed through a heat exchanger to reach 99ºC. All the smooth lines in Figure

10 represent simulations run with the condenser temperature fixed at 40ºC. The process design criteria (Table 8) clearly says that the discharge temperature from this unit has to be 20ºC, which is why another simulation was run with the correct outlet conditions. The results from this run are depicted with a dashed line and also takes into account a pressure drop.

The reboiler duty was not significantly affected by the changes in column heights (see Appendix D – Stripper dimensioning), which is why it was chosen to pursue with the shortest of the column heights analyzed in this section, i.e. 9 m. The corresponding column diameter of this column height is 6.33 m. Looking at the temperature profile trend in the picture below indicates that isothermal zones are avoided with shorter the stripper column heights, hence, it could have been possible to choose a column height as short as 7 m. However, since it was not known how much the column diameter would need to be altered (reduced or increased) due to the following stripper configurations, the shorter column heights were discarded for the stripper column in this study. Even if it would have meant a lower capital cost for the capture plant.
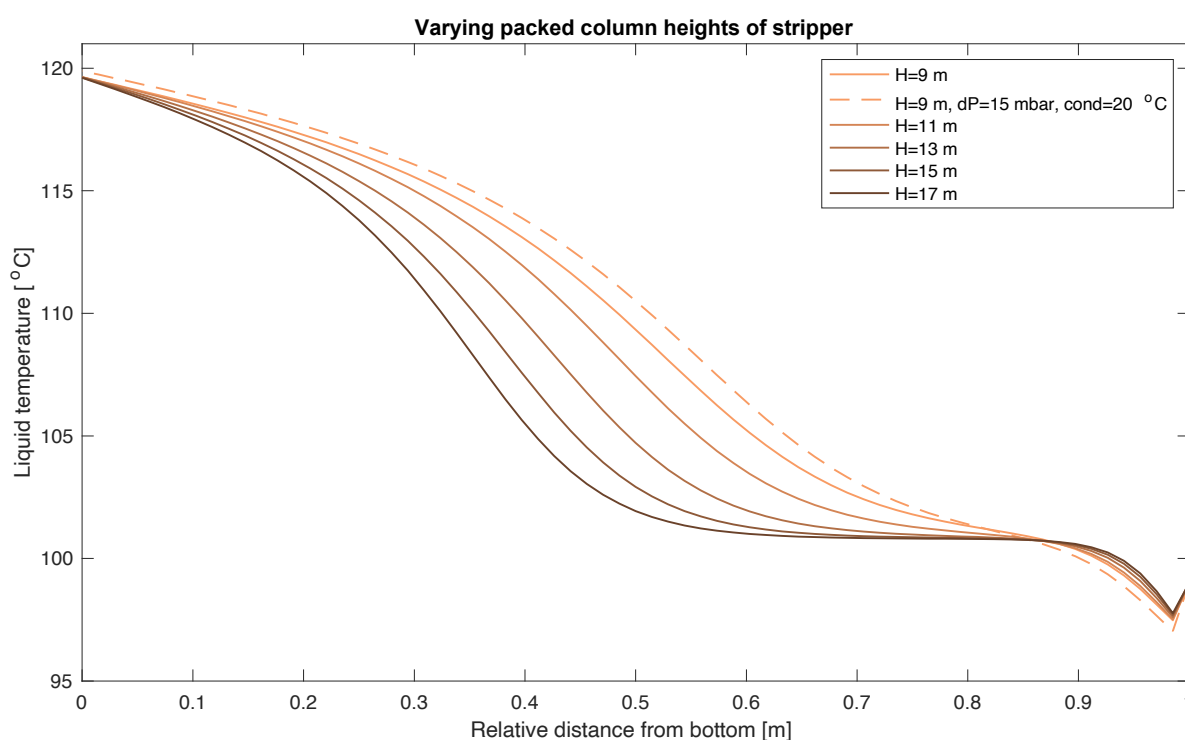
Figure 10 Varying packing heights of the stripper column with fixed solvent flow rate.

5.4. Standard MEA process

Some of the design parameters (flue gas and solvent temperature at absorber inlet, CO_2 gas temperature at reflux outlet, MEA concentration at washer outlet) presented in Table 8 were selected on basis of the design specifications for capture plants in the CO2stCap project (Biermann et al., 2018; Garðarsdóttir et al., 2018). The absorber, washer and stripper operating pressure, pressure drop, packing height and diameter were defined in the previous chapter.

Table 8 Main design parameters for the standard MEA process.

Flue gas CO_2 capture rate (wt%)	90
Absorber top stage pressure (bar)	1
Absorber pressure drop (bar)	0.025
Absorber packing height (m)	14
Absorber packing diameter (m)	11
Washer top stage pressure (bar)	1
Washer pressure drop (bar)	0.004
Washer packing height (m)	5.4
Washer packing diameter (m)	11
Stripper top stage pressure (bar)	1.8
Stripper pressure drop (bar)	0.015
Stripper packing height (m)	9
Stripper packing diameter (m)	6.6
MEA concentration (wt%)	30
Flue gas temperature at absorber inlet (ºC)	40
Lean solvent temperature at absorber inlet (ºC)	40
Rich solvent temperature after Heat-X (ºC)	107
Rich solvent temperature at stripper inlet (ºC)	99
Rich solvent feed stage in stripper	2
Reboiler temperature	121
CO_2 gas temperature at condenser outlet (ºC)	20
Lean CO_2 loading (mol CO_2/mol MEA)	0.25
MEA concentration at washer outlet (ppm)	<1

Figure 11 Aspen Plus flowsheet of the base case capture process with MEA.
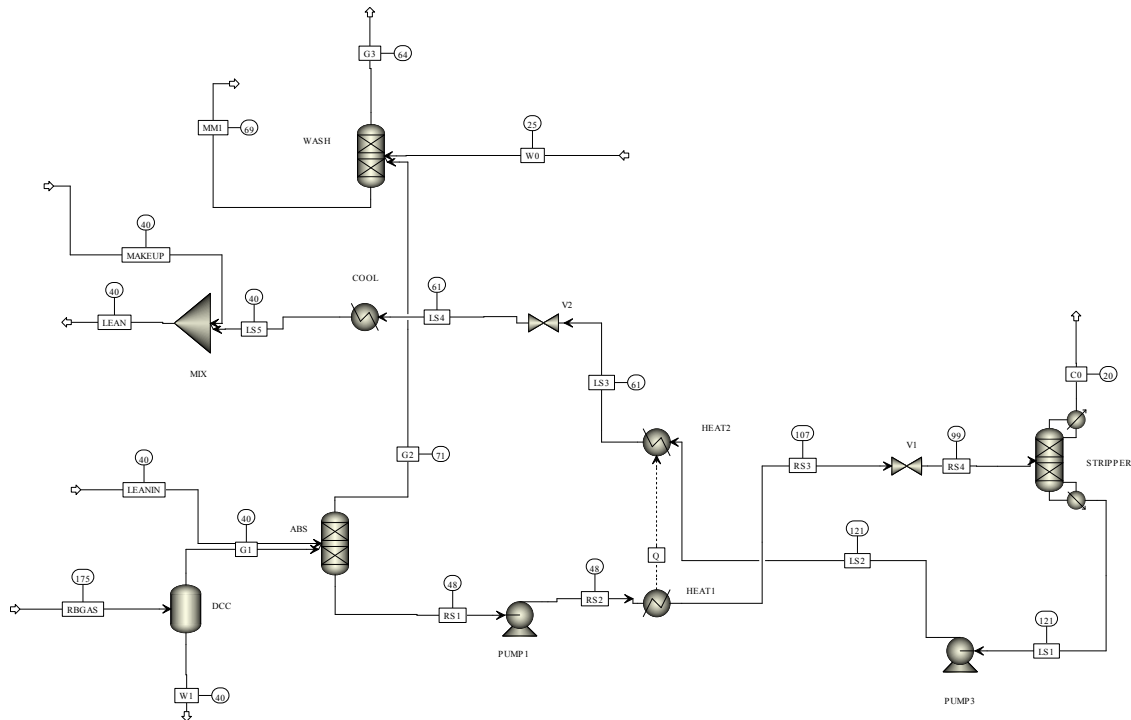
As is shown in Figure 11, the absorber was modelled with two RadFrac blocks with packed columns where the carbon capture is designated to happen mainly in ABS and the MEA slip from that unit is captured in WASH. The stripper is modelled with one partial condenser (top stage), a packed column and one kettle reboiler (bottom stage) inbuilt in the RadFrac block.

5.5.   Modified MEA process

The modified MEA process comprises a stripper overhead compression configuration (Figure 12). Different compressor discharge pressures (4–10 bar) were evaluated at different stripper operating pressures (1–1.8 bar). The maximum operating pressure of the stripper with this model is around 1.8 bar. This pressure guarantees that the reboiler temperature will not exceed that of the MEA solvent degradation temperature, i.e. 122ºC. Heat integration with this process modification is possible when the excess heat available in Q1 (through condensation of the CO_2/H_2O vapor) is redirected to the stripper reboiler. It was attempted to transfer the excess heat available in this manner in Aspen Plus, however, it was not successful. Therefore, the decreased reboiler duty due to heat integration was accounted for in the final calculations by manually deducting the amount of heat released (when Q1 discharge temperature=reboiler temperature) from the reboiler duty.
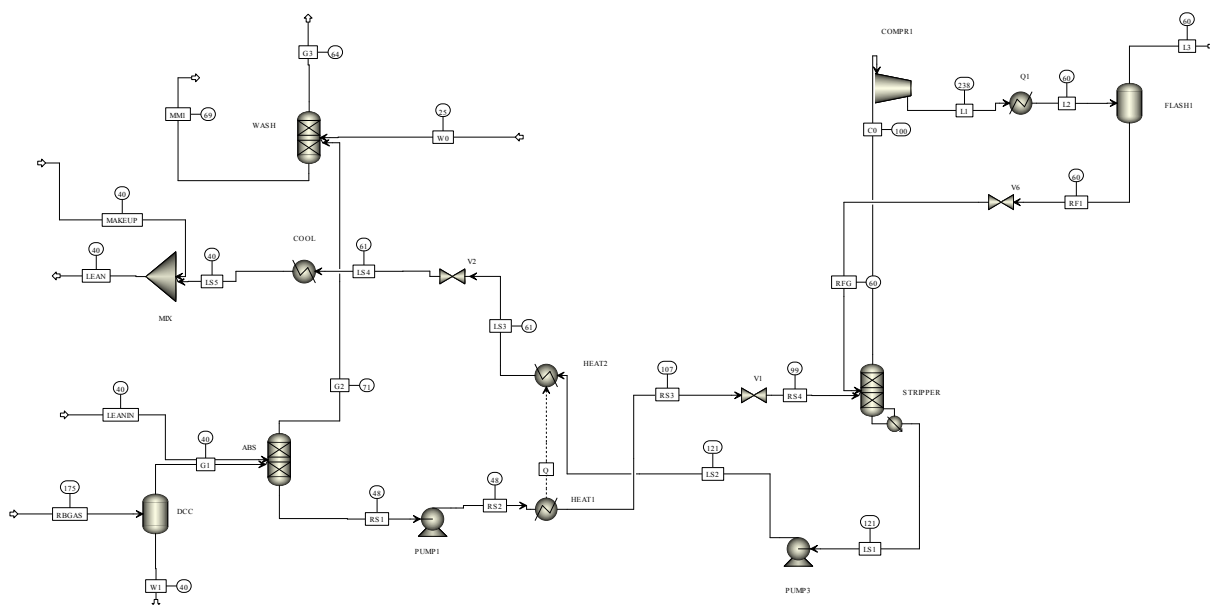
Figure 12 Aspen Plus flowsheet of the modified case capture process with MEA. The design alteration from the standard case is the addition of a compressor prior to the heat exchanger in the condenser arrangement of the stripper. Case 1 is illustrated here with a 6 bar discharge pressure compressor.

Three cases were studied as listed in Table 9. The temperature of the CO_2 gas leaving the condenser remained the same, 60ºC, for the three cases. The solvent temperature at the stripper inlet needed to be changed manually, considering the minimum temperature approach (10ºC) and the reboiler temperature. The pressure drop, height and diameter of the stripper packing had to be altered when decreasing the stripper pressure in order to meet the 90 wt% capture rate while minimizing hydraulic issues in the column, i.e. flooding and weeping. Other important design parameters were kept the same as in Table 8.

Four versions of the modified stripper were evaluated even further after finding valuable correlations from the case 1–3 results. The condenser discharge temperature was fixed at 20ºC in these configurations. Also, an additional heat exchanger was added between one of the valves (V6) and the stripper to increase the rich solvent temperature from 20ºC to ca 98ºC. Doing so ensures a more efficient desorption process. One more heat exchanger with 99ºC discharge temperature was added between V1 and the stripper for the last two flowsheet configurations with 1.3 bar stripper operating pressure. Q1 is the heat source (theoretical assumption) for the additional heat exchangers.

Table 9 Major changes of design parameters in the capture plant due to different stripper pressures in the configuration cases 1-3.

	Case 1	Case 2	Case 3
Stripper top stage pressure (bar)	1.8	1.3	1.0
Stripper pressure drop (bar)	0.015	0.015	0.02
Stripper packing height (m)	9	9	10.5
Stripper packing diameter (m)	7.4	8.5	10
Rich solvent temperature after Heat-X (ºC)	107	100	93
Rich solvent temperature at stripper inlet (ºC)	99	92	85
Reboiler temperature (ºC)	121	112	104

In order to add a compressor to the reflux loop, the inbuilt partial condenser in the RadFrac model had to be reconstructed. This was done by connecting the outlet gas stream from the stripper column to a cooler (COND in Figure 13), with the resulting stream entering a flash vessel (which splits the stream into a pure vapor and liquid stream respectively) and then connecting the liquid stream from the flash outlet to a pump that leads the condensate back to the top stage of the stripper column. The reflux ratio is adjusted by tuning the vapor fraction parameter in the flash block. The external partial condenser was validated by comparing the stripper reboiler duty, condenser duty, flow rate, temperature and composition of the exiting stripper streams with that of a stripper model with an inbuilt partial condenser. Results from this validation step are presented in Appendix E – Validation of external partial condenser.
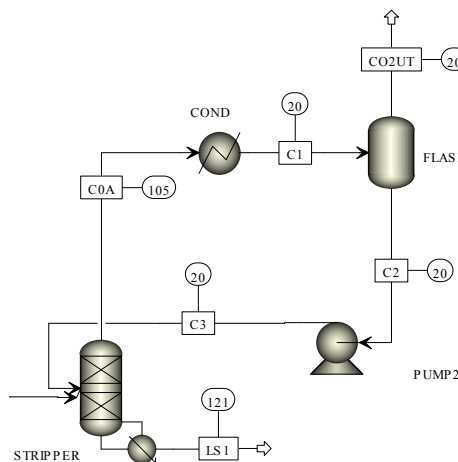
Figure 13 External partial condenser for the stripper. The inbuilt condenser of the RadFrac block was replaced with an external reflux loop equipped with a heat exchanger and a flash block.

26

CO_2 compression is needed to comply with pipeline specifications for CO_2 transport, around 95% pure CO_2 (Hasan et al., 2012), and stands for the highest exergy losses during operation of a Post-CC plant, after the absorption/desorption stages. According to literature (Ferrara et al., 2017; Kuramochi et al., 2012), compressors used for the liquification of CO_2 are usually modelled with 80–85% isentropic efficiency and 90–99% mechanical efficiency. The isentropic efficiency and mechanical efficiency of the compressors in this study were set at 80% and 97% respectively. Larger efficiency values result in less exergy losses.

6. Results and discussion

The heat/power production and consumption values reported throughout this chapter are in alignment with 90% carbon capture rate of the recovery boiler flue gas from a pulp mill with a yearly pulp production capacity of 700 000 ADt. This corresponds to 135 t_{CO2} per hour and 1.06 Mt_{CO2} per year, assuming 7840 equivalent full-load hours per year.

6.1.   Standard MEA process

Since both condenser and reboiler are inbuilt in the RadFrac model with this configuration, their heat duty was directly derived from the simulation results in the stripper block. The MEA slip presented in Table 10 Performance of a standard process with different number of segments in the absorber. corresponds to the MEA concentration (mole basis) in the gas stream leaving the stripper condenser. Increasing the number of segments from 10 to 70 in the stripper packing required a reduction of the column diameter from previous 7.4 to 6.8 m in order to keep the capture rate at 90 wt%. Changing from model I to II also required further reduction of the column diameter, but mainly to avoid disturbances in the column hydraulics.

Table 10 Performance of a standard process with different number of segments in the absorber.

Model	Performance	Number of segments	
		10	70
I	Reboiler duty (MW$_{th}$)	171	155
	Condenser duty (MW$_{th}$)	-54.1	-37.4
	MEA slip (ppm)	$1.71 \cdot 10^{-5}$	$1.03 \cdot 10^{-5}$
II	Reboiler duty (MW$_{th}$)	159	155
	Condenser duty (MW$_{th}$)	-41.2	-37.4
	MEA slip (ppm)	$1.10 \cdot 10^{-5}$	$8.68 \cdot 10^{-6}$

The performance results presented here indicate that there is no significant difference in the heat duties between model I and II when the packing section of the stripper model is discretized with 70 discretization points along its axial domain. Any difference between the models will only affect the desorption process in the packing column and, since that part is not the main feature of interest in the process modification, it was decided to proceed with model I and 70 segments from here on. There is a very small difference though, regarding the traces of MEA in the exiting gas stream. This disagreement is negligible.

6.2.   Modified MEA process

Decreasing the stripper pressure may be beneficial for heat integration but doing so results in a higher steam consumption in regard to the solvent regeneration process. The increased reboiler duty when reducing the stripper pressure is mainly due to the increased need of vapor in the desorption process, since the feed temperature is limited by the reboiler temperature (through the minimum temperature approach in the simplified cross heat-exchanger), which is lower at lower operating pressures. The lower feed temperature means that the incoming rich solvent has less amount of free CO_2 in the liquid phase. Hence, increasing the vapor concentration is needed in the stripper column in order to compensate for the constrained material transfer of CO_2 from the liquid to the gaseous phase of the stripper feed.
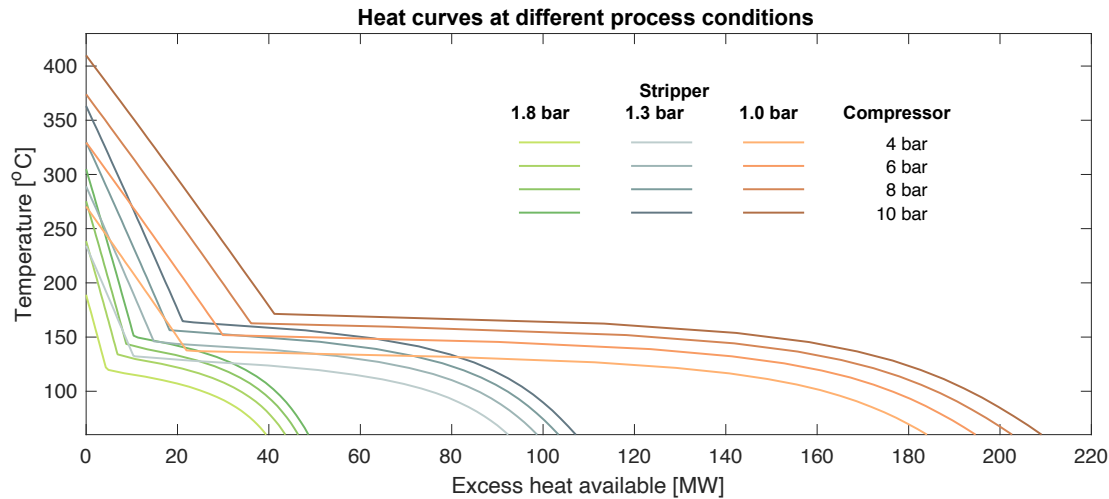
Figure 14 Potential thermal energy output from case 1–3 with the vapor compression configuration.

Figure 14 shows that increasing the discharge pressure of the compressor results in more heat available upon condensation of the leaving gas stream. However, a lower operating stripper pressure means higher discharge temperatures from the compressor outlet. Operating at such high temperatures can be detrimental for the equipment if they are not appropriately designed for such extreme conditions. Equipment that can handle higher temperatures is usually a lot more expensive. Therefore, regardless of how much more excess heat available is achieved with larger compressor discharge pressures and lower stripper operating pressures, it is important to take this detail in consideration when dealing with stripper overhead compression configurations. More results from Case 1–3 are presented in Table 11. However, the thermal energy available from the condensation step is not deducted from the reboiler duties, Q_{reb}, reported in this table.

Table 11 Obtained simulation results for Case 1–3, listed from top to bottom.

P0 (bar)	Pa (bar)	Ta (°C)	Tb (°C)	Compression work (MW)	MEA (ppm)	Qreb (MW)	Qreb (GJ/t$_{CO2}$)	Reboiler T (°C)	p(H$_2$O)
	4	189	60	5.69	444	154	4.10	121	0.857
1.8	6	238	60	9.01	452	154	4.10	121	0.860
	8	275	60	11.5	451	154	4.11	121	0.860
	10	305	60	13.6	451	154	4.11	121	0.860
	4	234	60	13.6	853	196	5.23	112	0.879
1.3	6	289	60	19.4	852	196	5.23	112	0.879
	8	330	60	23.8	851	196	5.23	112	0.879
	10	363	60	27.4	850	196	5.23	112	0.878
	4	270	60	28.6	900	274	7.29	104	0.804
1	6	329	60	38.8	899	274	7.29	104	0.804
	8	374	60	46.6	898	274	7.29	104	0.803
	10	410	60	53.0	897	274	7.29	104	0.803

These results indicate that alteration of the stripper operating pressure has a larger effect than what the compressor discharge pressure has on the resulting compression work, MEA slip, reboiler duty, reboiler temperature and the water partial pressure in the compressor gas inlet (p(H2O)). P0 denotes the stripper operating pressure, Pa is the compressor discharge pressure, Ta is the compressor discharge temperature and Tb is the condenser discharge temperature. Since the Ta value in all cases studied in this section is larger than the MEA degradation temperature, it means that one can assume that all the MEA slip will go to waste, regardless of a stripper reflux. Significant amounts of MEA slip can be reduced by having a wash section on the stripper head before the gas gets compressed. The specific reboiler duty increases from ca. 4.1 to 7.3 GJ/t_{CO_2} when reducing the stripper operating pressure from 1.8 bar to 1.0 bar. Figure 15 showcases an overview of the energy produced and consumed in the modified MEA process with different operating pressures of the stripper.
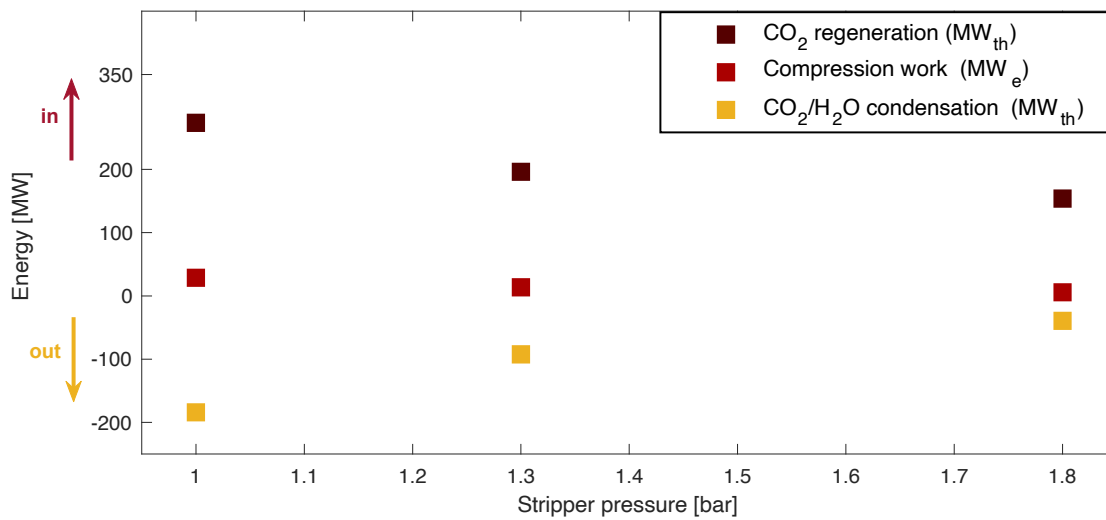
Figure 15 Energy input/output versus operating pressure in terms of thermal energy made available (CO₂/H₂O condensation), steam consumption (CO₂ regeneration process) and electricity consumption (compression). The vapor compression discharge pressure is 4 bar in this example.

The overhead compression configuration was further evaluated with heat integration at two different stripper operating pressures (1.3 and 1.8 bar), with the same outlet conditions as in the baseline case. In this study, the steam conservation potential is defined as the net consumption reduction with respect to the reboiler duty in the standard configuration, see Appendix F – Steam conservation potential for a calculation example. The simulation results (Table 12) indicate that increasing the compressor discharge pressure with 1 bar increases the steam conservation potential in both cases. The first compressor in the compression train usually has a discharge pressure of around 4 bar (Onarheim et al., 2017), and since the CO₂/H₂O gas stream exiting from the modified stripper will already be pressurized means that one less compression step is needed when comparing to the standard configuration. Neglecting the electricity consumption due to the overhead compressor can lead one to think that the stripper operating at lower pressure, combined with the higher discharge pressure, results in the largest steam conservation potential (24% as shown in Table 12). At least when comparing just these four examples with each other.

Table 12 Calculations of primary steam demand and steam conservation potential for different versions of the stripper overhead compression configuration. The steam conservation potential indicates a net consumption reduction with respect to the heat duty in the standard configuration.

Energy sink		Stripper pressure (bar)			
		1.3		1.8	
		Compressor discharge pressure (bar)			
		4	5	4	5
Reboiler	Heat duty (MW$_{th}$)	-196	-196	-153	-153
	Heat from condensation (MW$_{th}$)	+60	+79	+5	+15
	Steam demand (MW$_{th}$)	-136	-117	-148	-138
	Steam conservation (MW$_{th}$)	19	37	6	16
	Steam conservation (%)	12	24	4.1	11
Overhead compressor	Electricity duty (MW$_e$)	-14	-18	-6	-8
Thermodynamic energy efficiency potential		1.32	2.12	1.09	2.14

However, the electricity provided by a pulp mill is most probably produced internally through conversion of superheated steam. The ratio of energy output and energy input is commonly used to measure energy efficiency (Forsström et al., 2011). Considering the additional electricity demand will be relevant if the intention is to maximize the energy efficiency. In this case, the energy output is represented as the savings in steam consumption due to heat integration and the energy input as the compression work. Taking the thermodynamic energy efficiency potential into account indicates that the optimal case among those presented in Table 12 is the 1.8-bar stripper equipped with an overhead compressor with 5 bar discharge pressure. This modification may lead to savings of up to 11% in primary steam consumption and will require one less compression step in the downstream purification process, relative to the standard MEA process configuration.

7. Conclusion

A MEA-based chemical absorption and desorption process was rigorously modelled in Aspen Plus with a rate-based approach and validated against experimental data. A good agreement was achieved between the simulation results and experimental data in the absorber validation, with no more than 1.9% error in the estimation of the CO_2 removal efficiency and 4.1% error in the rich loading estimation. However, the results from the simulated stripper models did not coincide with experimental data to the same extent. The default rate-based setting was then altered, which reduced the estimated error of the reboiler duty from 22% to 6% for the UTA case. The predicted lean loading in the SINTEF case was not affected by the alternative rate-based model.

Different solvent flow rates were evaluated when dimensioning the columns to ensure efficient use of the entire packing. The minimum required packed column heights for the absorber and desorber in the standard MEA process were defined as 14 m and 9 m respectively, considering 90 wt% capture rate from the reboiler flue gas of a reference pulp mill with 700 000 ADt pulp production capacity per year. The specific reboiler duty needed to achieve this capture efficiency with 30 wt% MEA, $L=1.1L_{min}$ and 0.25 lean CO_2 loading in a standard MEA process configuration is 4.1 GJ/t_{CO2}.

Suitable temperature levels for heat integration, within and across the capture plant, were obtained by considering the heat consumed and excess heat made available in the MEA process. This was possible through an assessment of different versions of a stripper overhead compression configuration. The gas stream exiting the stripper is condensed to 20ºC before compression in the conventional MEA process. Compressing this stream and providing the reboiler with some of the higher quality heat, released from the water condensation, will decrease the steam flow rate drawn off from the steam cycle. However, at the cost of additional electricity needed for compression. Energy balance calculations were conducted for the modified MEA processes by considering both the steam conservation potential, with reference to the baseline case, and the theoretical energy efficiency potential.

The simulation results indicate that the configuration with a stripper operating pressure and compressor discharge pressure of 1.8 bar and 5 bar respectively may lead to savings of up to 11% in steam consumption, while cutting the need of one of compression step in the downstream purification process. The specific reboiler duty is 3.7 GJ/t_{CO2} with this version of stripper modification. The heat integration potential of the capture plant with a specific process in a Kraft pulp mill indicated energy savings in the same order of magnitude.Thereby, making the BECCS concept a more attractive environmental solution for the Swedish pulp and paper industry to mitigate climate change.

8. Future work

This chapter addresses some limitations of the study and suggests alternative approaches of relevance to future work in this area.

8.1. Aspen Plus model

The fact that the MEA solvent is not completely recirculated and that no chemical reactions are considered for the MEA degradation is a drawback with this simulation. Solvent degradation reactions should be included when modelling the MEA process since it may have a relevant role in the economics and operation of the capture system as a whole. Another property package should be used for processes operating at 10 bar or higher, since the ENRTL model gives accurate results up to medium pressures only. The CO_2 compression section should be modelled separately, using the Predictive Soave-Redlich-Kwong (PSRK) property method instead since it is generally more accurate for systems without water present at high pressures (Adams & Barton, 2010). Ultimately, the mass and energy balances in the condenser and compressors are of main importance when analyzing the energy conservation potential. Choosing a thermodynamic package that supports higher validity in the compression and condenser stream results, over the one used in this study (mainly relevant for non-ideal electrolyte liquid solutions), is justifiable since the streams in those process steps consists of mainly CO_2 and H_2O.

The results from the stripper model validation was less accurate than that of the absorber model validation in terms of how well they match experimental data. It is important to remember that, out of 48 campaign runs in the UTA plant and out of 19 campaign runs in the SINTEF plant, only one from each plant was run through the Aspen model. An improvement of the validation part in this study can be made by also reproducing all the other runs (or at least those runs that differ in operating conditions) of each plant. Doing so will give more confidence to the validity and reliability of the simulation results. Heat losses from the absorber and stripper columns were not accounted for in the simulation results either. Adding this detail in the model calculations will further increase the reliability of the stripping performance results.

8.2. Carbon capture design

The most relevant parameters that should be tuned in a continued version of this study are listed below. These are parameters that were kept constant throughout the evaluation of the modified stripper configuration. Tuning some of these as an attempt to reach a more optimized process design could be beneficial for a pulp mill integrated with carbon capture in terms of operational cost. The partial capture concept is especially important to consider in the process integration of carbon capture in integrated Kraft pulp and paper mills, since these normally lack steam surplus. Potential investors in the near future may perceive such an approach as more technical and economically feasible in retrofit projects. Extra emphasis should therefore be put on the capture rate by drawing up justifiable partial capture scenarios.

- Position of rich solvent feed
- Lean solvent loading
- Solvent flow rate
- Capture rate

References

Abdul Manaf, N., Qadir, A., Sharma, M., Parvareh, F., Milani, D., & Abbas, A. (2016). *Model-based optimisation of highly-integrated renewables with post-combustion carbon capture processes*.

Adams, T. A. (2018). *Learn Aspen Plus in 24 hours*. McGraw Education.

Adams, T. A., & Barton, P. I. (2010). High-efficiency power production from coal with carbon capture. *AIChE Journal*, *56*(12), 3120–3136. https://doi.org/10.1002/aic.12230

Ahn, H., Luberti, M., Liu, Z., & Brandani, S. (2013). Process configuration studies of the amine capture process for coal-fired power plants. *International Journal of Greenhouse Gas Control*, *16*, 29–40.

Aspen Technology, Inc. (2014). *Rate-Based Model of the CO_2 Capture Process by MEA using Aspen Plus*. Bedford, MA.

Batoon, V., Hicks, D., Huang, I., Hofmann, T., Kniep, J., Paulaha, C., Westling, E., & Merkel, T. (2019, August 29). *Scale-Up and Testing of Advanced Polaris Membrane CO_2 Capture Technology (DE-FE0031591)*.

Biermann, M., Normann, F., Johnsson, F., & Skagestad, R. (2018). Partial Carbon Capture by Absorption Cycle for Reduced Specific Capture Cost. *Industrial & Engineering Chemistry Research*, *57*(45), 15411–15422. https://doi.org/10.1021/acs.iecr.8b02074

BMU Austria. (1995). *Sector Waste Management Concept for Paper and Pulp Industry. Prevention-Utilisation-Disposal*. Ministry of Environment.

Bottoms, R. R. (1931). Organic Bases for Gas Purification. *Industrial & Engineering Chemistry*, *23*(5), 501–504. https://doi.org/10.1021/ie50257a007

Bravo, J.L., Rocha, J. A., & Fair, J. R. (1985). Mass transfer in gauze packings. *Hydrocarbon Process*, *64*, 91–95.

Bravo, J.L., Rocha, J. A., & Fair, J. R. (1992). A comprehensive model for the performance of columns containing structured packings. *Industrial & Engineering Chemistry Research*, *128*, A439-457.

Bui, M., Adjiman, C. S., Bardow, A., Anthony, E. J., Boston, A., Brown, S., Fennell, P. S., Fuss, S., Galindo, A., Hackett, L. A., Hallett, J. P., Herzog, H. J., Jackson, G., Kemper, J., Krevor, S., Maitland, G. C., Matuszewski, M., Metcalfe, I. S., Petit, C., … Mac Dowell, N. (2018). Carbon capture and storage (CCS): The way forward. *Energy & Environmental Science*, *11*(5), 1062–1176.

Bui, M., Gunawan, I., Verheyen, V., Feron, P., Meuleman, E., & Adeloju, S. (2014). Dynamic modelling and optimisation of flexible operation in post-combustion CO_2 capture plants—A review. *Computers & Chemical Engineering*, *61*, 245–265. https://doi.org/10.1016/j.compchemeng.2013.11.015

Conference on Mathematical Modelling, & Troch, I. (Eds.). (2009). *Proceedings / MATHMOD 09: 6th Vienna Conference on Mathematical Modelling, Vienna, February 11 - 13, 2009, Vienna University of*

Technology, Austria ; abstract volume. ARGESIM, Publ. House.

Dugas, R. (2006). *Pilot plant study of carbon dioxide capture by aqueous monoethanolamine*.

Errico, M., Madeddu, C., Pinna, D., & Baratti, R. (2016). Model calibration for the carbon dioxide-amine absorption system. *Applied Energy*, *183*, 958–968.

Ferrara, G., Lanzini, A., Leone, P., Ho, M. T., & Wiley, D. E. (2017). Exergetic and exergoeconomic analysis of post-combustion CO_2 capture using MEA-solvent chemical absorption. *Energy*, *130*, 113–128. https://doi.org/10.1016/j.energy.2017.04.096

Forsström, J., Lahti, P., Pursiheimo, E., Rämä, M., Shemeikka, J., Sipilä, K., Tuominen, P., & Wahlgren, I. (2011). *Measuring energy efficiency: Indicators and potentials in buildings, communities and energy systems*. VTT.

Fosbøl, P. L., Gaspar, J., Ehlers, S., Kather, A., Briot, P., Nienoord, M., Khakharia, P., Le Moullec, Y., Berglihn, O. T., & Kvamsdal, H. (2014). Benchmarking and Comparing First and Second Generation Post Combustion CO_2 Capture Technologies. *Energy Procedia*, *63*, 27–44.

FRBC. (2010). *NOx emissions from recovery boilers – why discrepancy between Finnish and Swedish values* (22.12.2010, p. 12). Finnish Recovery Boiler Committee.

Freguia, S., & Rochelle, G. T. (2003). Modeling of CO_2 capture by aqueous monoethanolamine. *AIChE Journal*, *49*(7), 1676–1686. https://doi.org/10.1002/aic.690490708

Fuss, S., Jones, C. D., Kraxner, F., Peters, G. P., Smith, P., Tavoni, M., van Vuuren, D. P., Canadell, J. G., Jackson, R. B., Milne, J., Moreira, J. R., Nakicenovic, N., Sharifi, A., & Yamagata, Y. (2016). Research priorities for negative emissions. *Environmental Research Letters*, *11*(11), 115007.

Garcia, M., Knuutila, H. K., & Gu, S. (2017). ASPEN PLUS simulation model for CO_2 removal with MEA: Validation of desorption model with experimental data. *Journal of Environmental Chemical Engineering*, *5*(5), 4693–4701. https://doi.org/10.1016/j.jece.2017.08.024

Garðarsdóttir, S. Ó. (2017). *Technical and economic conditions for efficient implementation of CO_2 capture: Process design and operational strategies for power generation and process industries*. Chalmers University of Technology.

Garðarsdóttir, S. Ó., Normann, F., Skagestad, R., & Johnsson, F. (2018). Investment costs and CO_2 reduction potential of carbon capture from industrial plants – A Swedish case study. *International Journal of Greenhouse Gas Control*, *76*, 111–124. https://doi.org/10.1016/j.ijggc.2018.06.022

Global CCS Institute. (2011). *Bio-energy with CCS*. https://www.globalccsinstitute.com/archive/hub/publications/25921/fact-sheet-3-bioccs-v4.pdf

Global CCS Institute. (2019). *The Global Status of CCS: 2019*.

Hammer, G., Lübcke, T., Kettner, R., Pillarella, M. R., Recknagel, H., Commichau, A., Neumann, H.-J., & Paczynska-Lahme, B. (2006). Natural Gas. In *Ullmann's Encyclopedia of Industrial Chemistry*. American Cancer Society. https://doi.org/10.1002/14356007.a17_073.pub2

Hanley, B., & Chen, C.-C. (2012). New mass-transfer correlations for packed towers. *AIChE Journal*, *58*(1), 132–152. https://doi.org/10.1002/aic.12574

Hasan, M. M. F., Baliban, R. C., Elia, J. A., & Floudas, C. A. (2012). Modeling, Simulation, and Optimization of Postcombustion CO_2 Capture for Variable Feed Concentration and Flow Rate. 1. Chemical Absorption and Membrane Processes. *Industrial & Engineering Chemistry Research*, *51*(48), 15642–15664. https://doi.org/10.1021/ie301571d

Haydary, J. (2018). *Chemical Process Design and Simulation: Aspen Plus and Aspen Hysys Applications*. John Wiley & Sons, Inc. https://doi.org/10.1002/9781119311478

Hektor, E. (2008). *Post-Combustion CO_2 Capture in Kraft Pulp Mills—Technical, Economic and System Aspects* [Chalmers University of Technology].
 https://research.chalmers.se/en/publication/74762

Hwang, J., Kim, J., Lee, H. W., Na, J., Ahn, B. S., Lee, S. D., Kim, H. S., Lee, H., & Lee, U. (2019). An experimental based optimization of a novel water lean amine solvent for post combustion CO_2 capture process. *Applied Energy*, *248*, 174–184. https://doi.org/10.1016/j.apenergy.2019.04.135

IEA. (2007). *Tracking Industrial Energy Efficiency and CO_2 Emissions*. OECD. https://doi.org/10.1787/9789264030404-en

IEAGHG. (2016). *Techno-Economic Evaluation of Retrofitting CCS in a Market Pulp Mill and an Integrated Pulp and Board Mill* (No. 2016/10).

IPCC. (2014). *Climate Change 2014 Mitigation of Climate Change: Working Group III Contribution to the Fifth Assessment Report of the Intergovernmental Panel on Climate Change*. Cambridge University Press. https://doi.org/10.1017/CBO9781107415416

Jönsson, J., & Berntsson, T. (2012). Analysing the potential for implementation of CCS within the European pulp and paper industry. *Energy*, *44*(1), 641–648.

Knudsen, J., Andersen, J., Jensen, J. N., & Biede, O. (2011). Results from test campaigns at the 1 t/h CO_2 post combustion capture pilot-plant in Esbjerg under the EU FP7 CESAR project. *1st Post Combustion Capture Conference*, 17–19.

Kuparinen, K., Vakkilainen, E., & Tynjälä, T. (2019). Biomass-based carbon capture and utilization in kraft pulp mills. *Mitigation and Adaptation Strategies for Global Change*, *24*(7), 1213–1230. https://doi.org/10.1007/s11027-018-9833-9

Kuramochi, T., Ramírez, A., Turkenburg, W., & Faaij, A. (2012). Comparative assessment of CO_2 capture technologies for carbon-intensive industrial processes. *Progress in Energy and Combustion Science*, *38*(1), 87–112. https://doi.org/10.1016/j.pecs.2011.05.001

Kvamsdal, H.M., & Rochelle, G. T. (2008). Effects of the Temperature Bulge in CO_2 Absorption from Flue Gas by Aqueous Monoethanolamine. *Industrial & Engineering Chemistry Research*, *47*(3), 867–875. https://doi.org/10.1021/ie061651s

Kvamsdal, H.M., Jakobsen, J. P., & Hoff, K. A. (2009). Dynamic modeling and simulation of a CO_2 absorber column for post-combustion CO_2 capture. *Chemical Engineering and Processing: Process Intensification*, *48*(1), 135–144. https://doi.org/10.1016/j.cep.2008.03.002

Le Moullec, Y., & Kanniche, M. (2011). Screening of flowsheet modifications for an efficient monoethanolamine (MEA) based post-combustion CO_2 capture. *International Journal of Greenhouse Gas Control*, *5*(4), 727–740. https://doi.org/10.1016/j.ijggc.2011.03.004

Lemaire, E., Bouillon, P. A., & Lettat, K. (2014). Development of HiCapt+ TM Process for CO_2 Capture from Lab to Industrial Pilot Plant. *Oil & Gas Science and Technology – Revue d'IFP Energies Nouvelles*, *69*(6), 1069–1080. https://doi.org/10.2516/ogst/2013153

Li, K., Leigh, W., Feron, P., Yu, H., & Tade, M. (2016). Systematic study of aqueous monoethanolamine (MEA)-based CO_2 capture process: Techno-economic assessment of the MEA process and its improvements. *Applied Energy*, *165*, 648–659. https://doi.org/10.1016/j.apenergy.2015.12.109

Luo, X., & Wang, M. (2017). Improving Prediction Accuracy of a Rate-Based Model of an MEA-Based Carbon Capture Process for Large-Scale Commercial Deployment. *Engineering*, *3*(2), 232–243. https://doi.org/10.1016/J.ENG.2017.02.001

Madeddu, C., Errico, M., & Baratti, R. (2018). Process analysis for the carbon dioxide chemical absorption–regeneration system. *Applied Energy*, *215*, 532–542.

Madeddu, C., Errico, M., & Baratti, R. (2019). *CO_2 Capture by Reactive Absorption-Stripping: Modeling, Analysis and Design*. https://doi.org/10.1007/978-3-030-04579-1

Marik Singh, S. K., Zabiri, H., Isa, F., & M. Shariff, A. (2017). Simulation of CO_2 Rich Natural Gas Pilot Plant Carbon Dioxide Absorption Column at Elevated Pressure Using Equilibrium and Rate Based Method. In M. S. Mohamed Ali, H. Wahid, N. A. Mohd Subha, S. Sahlan, M. A. Md. Yunus, & A. R. Wahap (Eds.), *Modeling, Design and Simulation of Systems* (Vol. 752, pp. 327–336). Springer Singapore. https://doi.org/10.1007/978-981-10-6502-6_29

Massimiliano, M., Madeddu, C., & Baratti, R. (2019). 4. Reactive absorption of carbon dioxide: Modeling insights. In F. I. Gómez-Castro & J. G. Segovia-Hernández (Eds.), *Process Intensification* (pp. 79–124). De Gruyter. https://doi.org/10.1515/9783110596120-004

Mclaren, D. (2012). A comparative global assessment of potential negative emissions technologies. *Process Safety and Environmental Protection*, *90*, 489–500. https://doi.org/10.1016/j.psep.2012.10.005

MTR. (n.d.). *CO_2 Removal from Syngas*. Membrane Technology & Research. Retrieved February 4, 2020, from https://www.mtrinc.com/our-business/refinery-and-syngas/co2-removal-from-syngas/

Muradov, N. Z. (2014). *Liberating energy from carbon: Introduction to decarbonization*. Springer.

Neveux, T., Le Moullec, Y., & Favre, É. (2017). Post-combustion CO_2 Capture by Chemical Gas-Liquid Absorption: Solvent Selection, Process Modelling, Energy Integration and Design Methods. In A. I. Papadopoulos & P. Seferlis (Eds.), *Process Systems and Materials for CO_2 Capture* (pp. 283–310). John Wiley & Sons, Ltd. https://doi.org/10.1002/9781119106418.ch11

Normann, F., Skagestad, R., Biermann, M., Wolf, J., & Mathisen, A. (2019). *CO2stCap—Reducing the Cost of Carbon Capture in Process Industry*. https://research.chalmers.se/publication/512527/file/512527_Fulltext.pdf

Øi, L. E. (2010). CO_2 removal by absorption: Challenges in modelling. *Mathematical and Computer Modelling of Dynamical Systems*, *16*(6), 511–533. https://doi.org/10.1080/13873954.2010.491676

Onarheim, K., Santos, S., Kangas, P., & Hankalin, V. (2017). Performance and costs of CCS in the pulp and paper industry part 1: Performance of amine-based post-combustion CO_2 capture. *International Journal of Greenhouse Gas Control*, *59*, 58–73. https://doi.org/10.1016/j.ijggc.2017.02.008

Puxty, G., & Maeder, M. (2016). The fundamentals of post-combustion capture. In *Absorption-Based Post-combustion Capture of Carbon Dioxide* (pp. 13–33). Elsevier. https://doi.org/10.1016/B978-0-08-100514-9.00002-0

Razi, N., Svendsen, H. F., & Bolland, O. (2013). Validation of mass transfer correlations for CO_2 absorption with MEA using pilot data. *International Journal of Greenhouse Gas Control*, *19*, 478–491. https://doi.org/10.1016/j.ijggc.2013.10.006

Regeringskansliet. (2017). *Klimatlag (2017:720)*. Miljö- och energidepartementet.

Reynolds, A. J., Verheyen, T. V., & Meuleman, E. (2016). Degradation of amine-based solvents. In *Absorption-Based Post-combustion Capture of Carbon Dioxide* (pp. 399–423). Elsevier. https://doi.org/10.1016/B978-0-08-100514-9.00016-0

Rootzén, J., Kjärstad, J., Johnsson, F., & Karlsson, H. (2018, May 22). *Deployment of BECCS in basic industry-a Swedish case study*.

Skagestad, R., Wolf, J., Anheden, M., Garðarsdóttir, S. Ó., Mathisen, A., & Normann, F. (2018, May 24). *Impact analysis of CO_2 capture from pulp mills—Effects on CO_2 emissions, costs and green electricity production*. International Conference on Negative CO_2 Emissions, Gothenburg, Sweden.
Smith, P., & Porter, J. R. (2018). Bioenergy in the IPCC Assessments. *GCB Bioenergy*, *10*(7), 428–431.

Solbraa, E. (2002). *Equilibrium and Non-Equilibrium Thermodynamics of Natural Gas Processing* (0809-103X; 2002:146) [Doctoral dissertation]. Norwegian University of Science and Technology.

Suhr, M., Klein, G., Kourti, I., Rodrigo Gonzalo, M., Giner Santonja, G., Roudier, S., Delgado Sancho, L., & Institute for Prospective Technological Studies. (2015). *Best Available Techniques (BAT) reference document for the production of pulp, paper and board*. Publications Office. http://dx.publications.europa.eu/10.2791/370629

Tobiesen, F. A., Juliussen, O., & Svendsen, H. F. (2008). Experimental validation of a rigorous desorber model for CO_2 post-combustion capture. *Chemical Engineering Science*, *63*(10), 2641–2656.

Tontiwachwuthikul, P., Meisen, A., & Lim, C. J. (1992). CO_2 absorption by NaOH, monoethanolamine and 2-amino-2-methyl-1-propanol solutions in a packed column. *Chemical Engineering Science*, *47*(2), 381–390. https://doi.org/10.1016/0009-2509(92)80028-B

Wolf, J. (2020, June 9). *Research Project Manager* [Personal communication].

ZEP, & EBTP. (2012). *Biomass with CO_2 Capture and Storage (Bio-CCS)—The way forward for Europe*. http://www.etipbioenergy.eu/images/EBTP-ZEP-Report-Bio-CCS-The-Way-Forward.pdf

Zhang, Y., & Chen, C.-C. (2013). Modeling CO_2 Absorption and Desorption by Aqueous Monoethanolamine Solution with Aspen Rate-based Model. *Energy Procedia*, *37*, 1584–1596. https://doi.org/10.1016/j.egypro.2013.06.034

Zhang, Y., Chen, H., Chen, C.-C., Plaza, J. M., Dugas, R., & Rochelle, G. T. (2009). Rate-Based Process Modeling Study of CO_2 Capture with Aqueous Monoethanolamine Solution. *Industrial & Engineering Chemistry Research*, *48*(20), 9233–9246. https://doi.org/10.1021/ie900068k

Zhang, Y., Que, H., & Chen, C.-C. (2011). Thermodynamic modeling for CO_2 absorption in aqueous MEA solution with electrolyte NRTL model. *Fluid Phase Equilibria*, *311*, 67–75. https://doi.org/10.1016/j.fluid.2011.08.025

Appendix A

Absorption validation: parameters and results

It was confirmed in a previous version of the absorber model validation within this project that the calculated performance values with regard to the absorber (rich loading and CO_2 removal %) coincide a bit better with corresponding experimental data with increasing number of segments. The simulation results presented in this part were therefore calculated using 50 segments for the packing section, i.e. the reactive absorber height is discretized in equal number of parts. The activity basis rate constants, k and E, are necessary input values for Aspen Plus to run the rate-based calculation with the power law expression. The values reported by Hikita et al. (1977) for reaction 4-5 and those by Pinsent et al. (1956) for reaction 6–7 are almost exclusively applied throughout all literature about modelling of the MEA process. However, not all studies disclose the exact values used and simply refer directly to the works of Hikita et al. (a) and Pinsent et al. (b) respectively. Some studies (Aspen Technology, Inc., 2014; Errico et al., 2016; Zhang & Chen, 2013) modified these values to fit different conditions, which is reasonable considering that the stripper operates at a higher temperature than the absorber for example.

Table A-1 Kinetic parameters, k and E, in Eq. (1) according to different sources.

| Reaction	k (kmol/m^{3}s)	E (cal/mol)	Notation	Reference
4	$3.020 \cdot 10^{14}$	9840.5	c	(Zhang & Chen (2013)
	$3.020 \cdot 10^{14}$	9855.8	d, g	(Aspen Technology, Inc., 2014), (Razi et al., 2013)
	$3.020 \cdot 10^{10}$	9840.5	e	(Luo & Wang, 2017)
	$9.770 \cdot 10^{10}$	9855.8	f	(Errico et al., 2016)
	$6.839 \cdot 10^{10}$	9855.8	f2	(Errico et al., 2016)
5 (both)	$3.230 \cdot 10^{19}$	15655	f	(Errico et al., 2016)
	$2.261 \cdot 10^{19}$	15655	f2	(Errico et al., 2016)
5 (absorber)	$5.520 \cdot 10^{23}$	16492	c2, e	(Zhang & Chen (2013), (Luo & Wang, 2017)
	$5.520 \cdot 10^{23}$	16518	d2	(Aspen Technology, Inc., 2014),
	$5.520 \cdot 10^{13}$	16518	g	(Razi et al., 2013)
5 (stripper)	$6.560 \cdot 10^{27}$	22748	c2, e	(Zhang & Chen, 2013), (Luo & Wang, 2017)
	$6.500 \cdot 10^{27}$	22782	d2	(Aspen Technology, Inc., 2014)
6	$1.330 \cdot 10^{27}$	13227	c, e	(Zhang & Chen, 2013), (Luo & Wang, 2017)
	$1.330 \cdot 10^{17}$	13249	d, g	(Aspen Technology, Inc., 2014), (Razi et al., 2013)
	$4.320 \cdot 10^{13}$	13249	f	(Errico et al., 2016)
7	$6.630 \cdot 10^{16}$	22748	c, e	(Zhang & Chen, 2013), (Luo & Wang, 2017)
	$6.630 \cdot 10^{16}$	25656	d, g	(Aspen Technology, Inc., 2014), (Razi et al., 2013)
	$2.380 \cdot 10^{17}$	29451	f	(Errico et al., 2016)

Table A-1 presents different kinetic parameter values reported in literature and from here on these sources will be referred to as c-f, according to their corresponding notation. All of them

ultimately origin from either a or b. Some values within the same category, i.e. reaction type, differ by several orders of magnitude. Notations with 2 at the end indicate that the value was adjusted with respect to a and b. Moreover, source e refers to c but it is worth noticing that the k value from these sources for reaction 4 differ from each other. This is most likely a typo since the same was noticed when comparing the k values of reaction 5 for the absorber from source g and d2. After all, source g claims to have taken their values straight from source d. In both cases, the difference is only in the exponential part. Even so, all of these different kinetic sets were evaluated as they were.

Table A-2 Henry's law constant parameters from different sources. T refers to the system temperature range in which these values are valid.

Component pairs	C_1	C_2	C_3	C_4	T (K)	Source
CO_2-H2O	100.650	-6147.7	-10.191	0	273–473	(Luo & Wang, 2017), (Aspen Technology, Inc., 2014)
CO_2-MEA	89.452	-2934.6	-11.592	0.01644	280-600	(Luo & Wang, 2017)
	20.3143	-896.5	0	0	0-2000	(Aspen Technology, Inc., 2014)

As explained in 5.1.1. Absorber, the Henry's law constants for CO_2 with water and MEA could not be obtained from the Aspen Plus databank, hence, they had to be found in literature (Table A-2). Contrary to the solubility of CO_2 in water, which has been well studied, there is relatively limited knowledge about the solubility of CO_2 in MEA (Zhang et al., 2011). Hereafter, the pilot-scale plant will be referred to as ABS1 and the lab-scale plant as ABS2. Figure A-1 i) and iii) shows the temperature profiles of the liquid phase in ABS1 and ABS2 respectively when using the Henry constants for CO_2-H_2O and CO_2-MEA from (Luo & Wang, 2017), e.
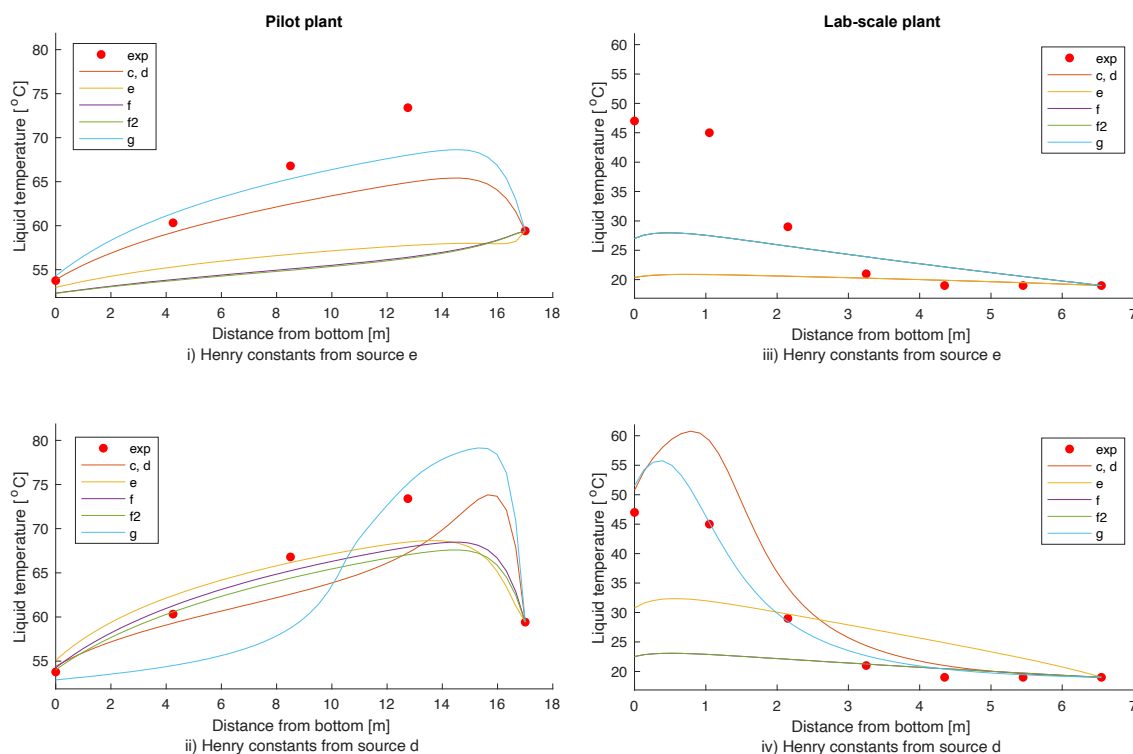
Figure A-1 Variation of the liquid temperature profile for ABS1 (i-ii) and ABS2 (iii-iv) using different kinetic and Henry's constant parameters.

Several of the simulation results are overlapping in Figure A-1 iii), hence only two lines are visible. c,d overlaps with the results from e, while f and f2 with g. Figure A-1 i) and iv) show the temperature profiles of the liquid phase in ABS1 and ABS2 respectively when using the Henry constants for CO_2-H_2O and CO_2-MEA from (Aspen Technology, Inc., 2014), d. In Figure A-1 iv), it becomes difficult to distinguish the simulation results from f, but in this example they are overlapping with the results from f2. When comparing all these four graphs, i-iv), it is clear that the Henry constants from d is the best option to continue with in the validation assessment, as its corresponding simulation results fits the experimental data from ABS1 and ABS2 better than that of e, without compromising the model accuracy. The simulation results using kinetic sets c and d are represented by the same line, yellow color, in the following two figures since they were only slightly different in regard to activation energy, E, and showed no significant difference of the temperature profiles upon graphical comparison.
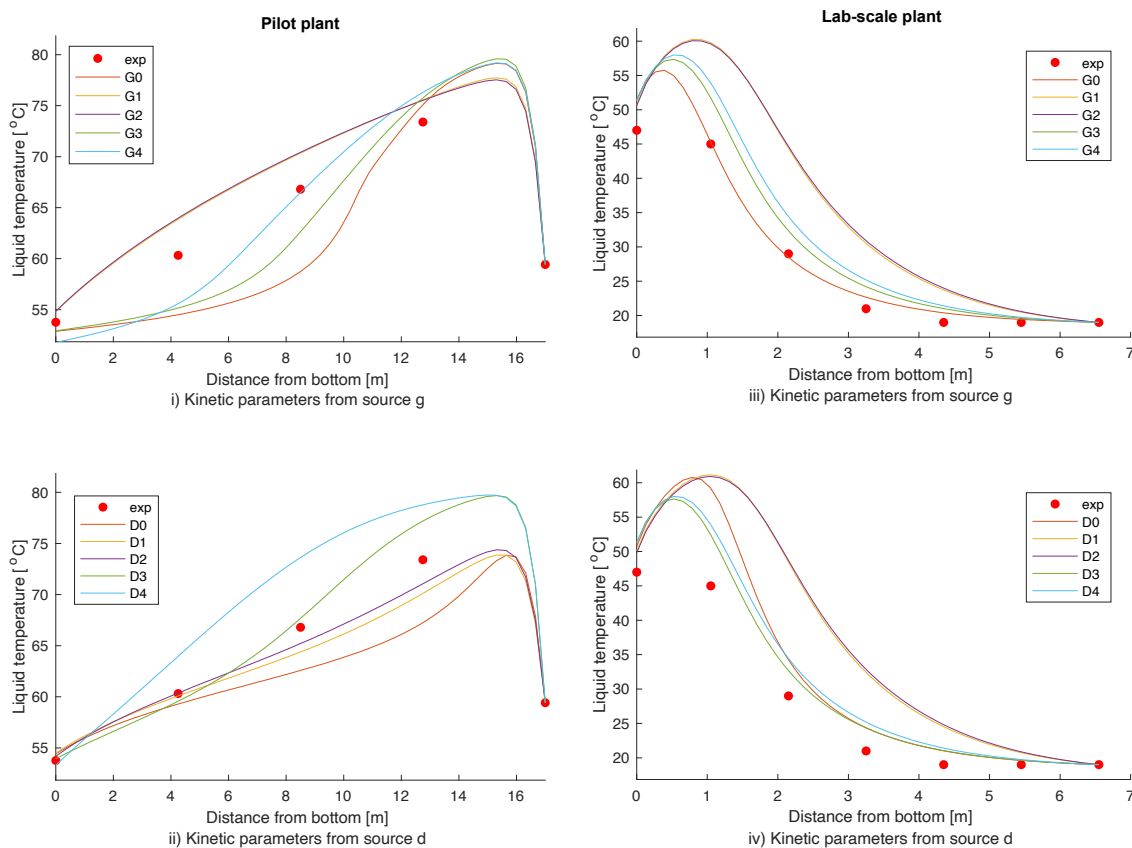
Figure A-2 Variation of the liquid temperature profile for ABS1 (i-ii) and ABS2 (iii-iv) for different combinations of kinetic parameters and interaction energy parameters.

The validation procedure continued by adjusting the GMENCC parameters in the Properties environment as shown in Table A-3, while keeping the Henry's constant parameters fixed according to source d. The 0 accompanying the upper-case letters, G and D, shows that the parameters were kept exactly as those automatically computed after selecting the ENRTL-RK method. The other values were retrieved from the sample simulation file "Rate-Based Model of the CO_2 Capture Process by MEA using Aspen Plus" through Exchange. Figure A-2 shows the temperature profiles of ABS1 (i-ii) and ABS2 (iii-iv) using different combinations of the energy interaction parameters. Overlapping occurs in these graphs, especially on i, iii and

iv, for changes 1-2 on the GMENCC parameters. The performance results of the absorbers using D0, D1 and D3 are tabulated in 5.1.1. Absorber.

Table A-3 Combinations of GMENCC parameters that relate to molecule-ion and ion-ion interactions.

Notation				Value	Molecule i or electrolyte i		Molecule j or electrolyte j		Value	Notation
D3, G3	D2, G2	D1, G1	D0, G0	9.888	H2O		MEAH+	MEACOO-	6.732	D4, G4
				-4.951	MEAH+	MEACOO-	H2O		-3.163	
				5.354	H2O		MEAH+	HCO3-	8.572	
				-4.071	MEAH+	HCO3-	H2O		-4.009	
				8.045	H2O		H3O+	HCO3-	8	
				-4.072	H3O+	HCO3-	H2O		-4	
				8.045	H2O		H3O+	OH-	8	
				-4.072	H3O+	OH-	H2O		-4	
				8.045	H2O		H3O+	CO3-2	8	
				-4.072	H3O+	CO3-2	H2O		-4	
				8	CO2		H3O+	OH-	8	
				-4	H3O+	OH-	CO2		-4	
				8	CO2		H3O+	HCO3-	8	
				-4	H3O+	HCO3-	CO2		-4	
				8	CO2		H3O+	CO3-2	8	
				-4	H3O+	CO3-2	CO2		-4	
				8	CO2		H3O+	MEACOO-	8	
				-4	H3O+	MEACOO-	CO2		-4	
				8	CO2		MEAH+	OH-	8	
				-4	MEAH+	OH-	CO2		-4	
				6	CO2		MEAH+	HCO3-	6	
				5.012	MEAH+	HCO3-	CO2		5.012	
				6	CO2		MEAH+	CO3-2	6	
				5.069	MEAH+	CO3-2	CO2		5.069	
				6	CO2		MEAH+	MEACOO-	6	
				5.072	MEAH+	MEACOO-	CO2		5.072	
				8	H2O		MEAH+	CO3-2	8	
				-4	MEAH+	CO3-2	H2O		-4	
				8	H2O		H3O+	MEACOO-	8	
				-4	H3O+	MEACOO-	H2O		-4	
				8	H2O		MEAH+	OH-	8	
				-4	MEAH+	OH-	H2O		-4	
				8	MEA		H3O+	OH-	8	
				-4	H3O+	OH-	MEA		-4	
				8	MEA		H3O+	HCO3-	8	
				-4	H3O+	HCO3-	MEA		-4	
				8	MEA		H3O+	CO3-2	8	
				-4	H3O+	CO3-2	MEA		-4	
				8	MEA		H3O+	MEACOO-	8	
				-4	H3O+	MEACOO-	MEA		-4	
				8	MEA		MEAH+	OH-	8	
				-4	MEAH+	OH-	MEA		-4	
				8	MEA		MEAH+	HCO3-	8	
				-4	MEAH+	HCO3-	MEA		-4	
				8	MEA		MEAH+	CO3-2	8	
				-4	MEAH+	CO3-2	MEA		-4	
				8	MEA		MEAH+	MEACOO-	8	
				-4	MEAH+	MEACOO-	MEA		-4	

Appendix B

Stripper validation: parameters and results

Table B-1 RadFrac parameters that were tuned in the stripper validation.

	Model I	Model II
Interfacial area factor	1	10
Heat transfer	1	5
Liquid mass transfer coefficient factor	1	3
Vapor mass transfer coefficient factor	1	10
Reaction condition factor	0.9	0.1
Interfacial area method	(Bravo et al., 1985)	(Hanley & Chen, 2012)

Table B-2 Error in the estimation of the lean loading with number of segments for the SINTEF plant.

Model	Performance	Number of segments			Experimental
		10	60	70	
I	Lean loading	0.253	0.251	0.251	0.219
	Error (%)	15	14	14	-
II	Lean loading	0.252	0.251	0.251	0.219
	Error (%)	15	14	14	-

Appendix C

Absorber dimensioning

Table C-1 Column parameters obtained from the design analysis of an absorber operating at 1 bar.

		Liquid flow rate (tonne/hr)	L/G ratio (kg/kg)	D (m)	H (m)	Base stage	No. of stages	Fixed pressure drop (mbar)	Theoretical max. pressure drop (mbar)
	Lmin	2190	3.4	10.7	100	3	100	0	-
1.05	Lmin	2298	3.5	10.9	25.4	6	100	0	-
1.1	Lmin	2408	3.7	11.0	14.2	8	100	0	-
1.1	Lmin	2408	3.7	11.0	14.0	7	100	25	29
1.15	Lmin	2517	3.9	discarded since it requires H/D <1 to obtain 90 wt% capture					
1.2	Lmin	2627	4.0						

The middle row in Table C-1 represents the column dimensions of the absorber used in the standard MEA process configuration.

Appendix D

Stripper dimensioning

Table D-1 Column parameters obtained from the design analysis of a stripper operating at 1.8 bar.

H (m)	D (m)	Capture rate (t_{CO2}/hr)	Qreb (MW)	Qreb (GJ/t_{CO2})	Reboiler T (K)	Limiting stage	Fixed pressure drop (mbar)	Theoretical max. pressure drop (mbar)	Condenser T (K)
17	6.28	135	150	3.99	394	69	0	-	313
15	6.31	135	150	3.98	394	69	0	-	313
13	6.31	135	149	3.98	394	69	0	-	313
11	6.30	135	149	3.98	394	69	0	-	313
9	6.30	135	149	3.98	394	69	0	-	313
9	6.33	135	150	4.01	394	69	15	18	293

The rich solvent flow rate entering the stripper is around 2440 tonne/hr and originates from the lean solvent flow rate (1.1Lmin) that enters the absorber unit. The bottom row in Table D-1 represents the column dimensions of the stripper used in the standard MEA process configuration.

Appendix E

Validation of external partial condenser

Table E-1 Validation results for the external partial condenser in the standard MEA process. The MEA concentration reported here concerns that in the gas stream exiting flash block.

	Absorber	Stripper	
Partial condenser		Inbuilt in RadFrac	External
No. of stages	10	10	10
Rich loading at absorber outlet	0.504		
Lean loading at stripper outlet		0.250	0.250
Boilup ratio		0.153	0.153
Stripper outlet gas stream temp (ºC)		105	105
Reboiler temp. (ºC)		121	121
MEA in product stream, ppm		$1.8 \cdot 10^{-5}$	$8.3 \cdot 10^{-5}$
Reboiler duty (MW$_{th}$)		172	172
Condenser duty (MW$_{th}$)		-54.4	-54.5

Appendix F

Steam conservation potential

This example relates to the calculation of the steam conservation potential resulting from heat integration in a modified MEA process with 1.8 bar stripper operating pressure and 5 bar compression discharge pressure. The quantity marked in red (Table 12) corresponds to the net heat required in the modified stripper, and the quantity marked in bold (Table 10) corresponds to the reboiler duty in the standard process configuration.

$$Steam\ conservation\ (\%) = \frac{-154.6 - (-\mathbf{138.22})}{-154.6} \times 100 \approx 11$$